

Review

Review of Structural Health Monitoring Techniques in Pipeline and Wind Turbine Industries

Vinamra Bhushan Sharma ^{1,†}, Kartik Singh ^{2,†}, Ravi Gupta ^{3,†} , Ayush Joshi ^{4,†} , Rakesh Dubey ¹, Vishwas Gupta ⁵, Shruti Bharadwaj ¹, Md. Iltaf Zafar ¹, Sushant Bajpai ^{5,*} , Mohd Ashhar Khan ², Anubhava Srivastava ¹, Divyang Pathak ² and Susham Biswas ^{1,*} 

- ¹ Department of Computer Science and Engineering, Rajiv Gandhi Institute of Petroleum Technology, Jais, Amethi 229304, India; pgi19002@rgipt.ac.in (V.B.S.); pgi19001@rgipt.ac.in (R.D.); pgi17001@rgipt.ac.in (S.B.); pgi15001@rgipt.ac.in (M.I.Z.); pgi18001@rgipt.ac.in (A.S.)
- ² Department of Chemical Engineering and Engineering Sciences, Rajiv Gandhi Institute of Petroleum Technology, Jais, Amethi 229304, India; Eche18020@rgipt.ac.in (K.S.); Eche18051@rgipt.ac.in (M.A.K.); Eche18013@rgipt.ac.in (D.P.)
- ³ Department of Computer Science and Engineering, CV Raman Global University, Bhubaneswar 752054, India; ravigupta19982010@gmail.com
- ⁴ Department of Petroleum Engineering, Oklahoma State University, Stillwater, OK 74077, USA; Ayush.joshi@okstate.edu
- ⁵ Department of Petroleum Engineering and Geological Sciences, Rajiv Gandhi Institute of Petroleum Technology, Jais, Amethi 229304, India; epe18056@rgipt.ac.in
- * Correspondence: epe18059@rgipt.ac.in (S.B.); susham@rgipt.ac.in (S.B.)
- † The authors contributed equally to this work.



Citation: Sharma, V.B.; Singh, K.; Gupta, R.; Joshi, A.; Dubey, R.; Gupta, V.; Bharadwaj, S.; Zafar, M.I.; Bajpai, S.; Khan, M.A.; et al. Review of Structural Health Monitoring Techniques in Pipeline and Wind Turbine Industries. *Appl. Syst. Innov.* **2021**, *4*, 59. <https://doi.org/10.3390/asi4030059>

Academic Editor: Luís Bragança

Received: 1 August 2021

Accepted: 24 August 2021

Published: 31 August 2021

Publisher's Note: MDPI stays neutral with regard to jurisdictional claims in published maps and institutional affiliations.



Copyright: © 2021 by the authors. Licensee MDPI, Basel, Switzerland. This article is an open access article distributed under the terms and conditions of the Creative Commons Attribution (CC BY) license (<https://creativecommons.org/licenses/by/4.0/>).

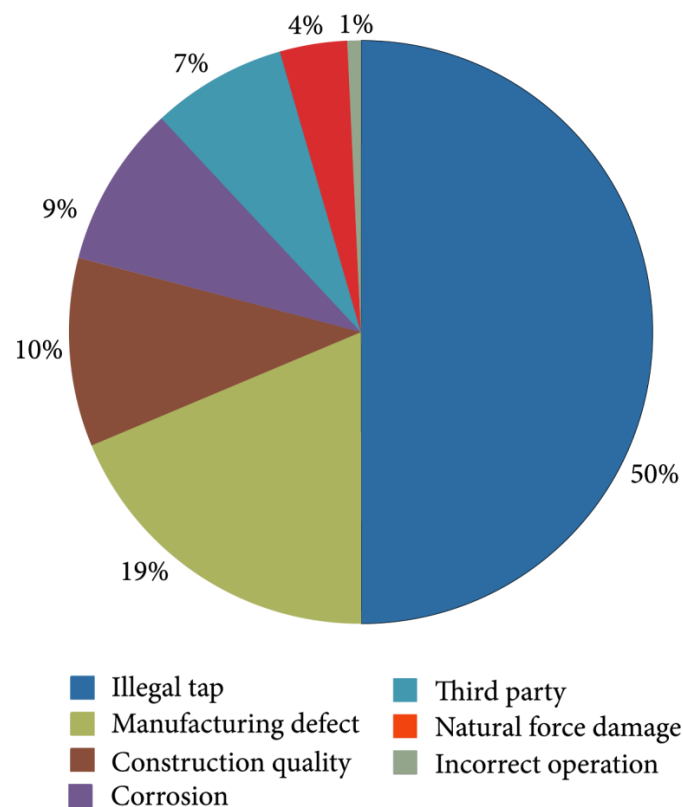
Abstract: There has been enormous growth in the energy sector in the new millennium, and it has enhanced energy demand, creating an exponential rise in the capital investment in the energy industry in the last few years. Regular monitoring of the health of industrial equipment is necessary, and thus, the concept of structural health monitoring (SHM) comes into play. In this paper, the purpose is to highlight the importance of SHM systems and various techniques primarily used in pipelining industries. There have been several advancements in SHM systems over the years such as Point OFS (optical fiber sensor) for Corrosion, Distributed OFS for physical and chemical sensing, etc. However, these advanced SHM technologies are at their nascent stages of development, and thus, there are several challenges that exist in the industries. The techniques based on acoustic, UAVs (Unmanned Aerial Vehicles), etc. bring in various challenges, as it becomes daunting to monitor the deformations from both sides by employing only one technique. In order to determine the damages well in advance, it is necessary that the sensor is positioned inside the pipes and gives the operators enough time to carry out the troubleshooting. However, the mentioned technologies have been unable to indicate the errors, and thus, there is the requirement for a newer technology to be developed. The purpose of this review manuscript is to enlighten the readers about the importance of structural health monitoring in pipeline and wind turbine industries.

Keywords: corrosion; sensors; structural health monitoring; unmanned aerial vehicles; energy industry

1. Introduction

For a long time, corrosion has been a major cause of concern in the oil and gas industry, proving to be fatal to production in a plethora of ways, including storage, transportation, infrastructure, production, and exploration [1–3], thereby causing a significant amount of loss to the industry. Hydrogen cracking also exhibits its catastrophic capabilities in oil and gas plants as it develops in various forms, leading to a loss of structural integrity of the plants. There are more than 528,000 km (328,000 miles) of natural gas transmission and gathering pipelines, and 119,000 km (74,000 miles) of crude oil transmission and gathering pipelines. The energy sector uses several infrastructures that are metallic and undergo

changes due to wear and tear and corrosion, leading to bending, breakage, leaks, and other damages (Scheme 1). Across more than two decades, the energy obtained through wind has gained enormous traction in the markets around the world, increasing from 2.4 to 11.4% in the EU between 2000 and 2015, which equals a 128.5 GW increase in use [4]. This is a result of the quick advances in the wind industry and the targets set by the European Union. The offshore placements of the wind farms have become unexpectedly the most profitable among all and produce more than all other renewable energy sources combined [5]. In Europe itself, 84 sites existed at the end of 2015 [6,7]. The structural health monitoring (SHM) systems play an important role in maximizing the potentials of the wind energy by increasing their life and efficiency through advanced monitoring. SHM allows for the identification of the damage and the implementation of those techniques. The basic causes of damage would include stresses, hysteresis, and wind or atmospheric erosions [8] not only in wind farms but also in other infrastructures associated with the generation of power and transportation in the energy sector; e.g., turbines, motors, pumps, and pipelines also require detailed inspection. Monitoring finds its applications in the civil, infrastructural, and aerodynamic fields, requiring some amount of studies for geometry and structures. The two major and most influential aspects that control the monitoring include the sensing technology and the interpretation algorithm that allows for information obtained from sensors to be converted into legible quantities that can in turn be used to provide the best solution manually or through technologies [9]. The basic elements of an ideal monitoring system would require the best measurements of damages and provide a reliable analysis in time to save and guard it from damages. The normalization and integration of data using the techniques of data science are the important aspects of processing for the SHM systems because the data received is basically in raw forms and needs to be utilized meaningfully. The preprocessed data are required to be worked on to extract the cracks, leaks, or structural damages or to predict future damages in structures [10].



Scheme 1. Damages and their types.

The key function of SHM is to maintain track of changes in the structural system's dynamic properties for detecting and locating damage, as well as to automatically determine whether the damage is harmful to the structure. Damage detection usually entails data processing to look for changes in structural dynamic characteristics (such as modal frequency, damping ratio, and mode shape) as well as inter-story drifts. Because structural damage results in a loss of stiffness, and the dynamic characteristics of a structure are directly connected to stiffness, it is reasonable to utilise natural frequency variations as a damage indicator. Changes in natural frequency are not always a reliable sign of damage, as the reaction of the damaged structure is nonlinear, and in most cases hysteretic, according to examinations of recorded data from structures. Furthermore, different environmental variables (for example, temperature) can alter the natural frequency of buildings without causing any structural harm (Scheme 1).

2. Health Monitoring Techniques in Pipeline Industry

2.1. In Pipeline Industry

Corrosion is a common phenomenon in places that contain oil. Recently, concentrations of corrosive substances have increased dramatically in crude oil. Materials such as sulfur and chloride and the increasing acidity are some of the common reasons. Several types of degradations inside refineries can take place with the varying environmental effects on naphthenic acids present in oils within the temperature range of 150–400 °C. These types include non-uniform, uniform, or localized pitting. This corrosion needs to be correctly and efficiently measured with the application of improvised techniques, and thereafter, the risk is to be calculated and minimized [11–14].

The production of fuel is also becoming increasingly difficult to this enhanced corrosive nature. The presence of corrosive elements in the oil is somewhat difficult to predict as it depends on a number of factors especially when it is caused by the naphthenic acids [15–20]. Some parameters that affect naphthenic acids corrosion are given in Table 1.

Table 1. The parameters that affect the naphthenic acids corrosion.

Parameter	Potential Target
Temperature	Up to 400 °C
Thickness Precision	0.05 mm
Spatial Resolution Precision	0.05 mm width and 0.05 mm length
Pipe Wall Thickness	3–25 mm
Pipe Diameter	>100 mm
Metallurgy	Low-Alloy Steel (<9% Cr & <2.5% Mo)

Hydrogen cracking is another common problem in the pipeline industry. It could also be termed as cold cracking or delayed cracking. In carbon or low-alloy steels, hydrogen cracking occurs as atomic hydrogen diffuses and forms molecular hydrogen in it. Molecular hydrogen formation can be facilitated by inclusions or trap sites. Hydrogen cracking may also occur in the absence of any tensile stress. Molecular hydrogen formation pressurizes the material internally and starts cracking. A hard brittle structure, hydrogen produced by welding, and the tensile stress that acts on the welding joint are the three major factors that give rise to cracking. Hydrogen cracking is also caused by hydrogen strain (change in dimension of the pipeline due to tensile stress). Hydrogen cracking is a form of embrittlement of hydrogen common to carbon steels that originates in a step-like way from the propagation and linkage of small laminar cracks resulting from hydrogen pressurization trap sites. The strain of the internal hydrogen pressure inside laminar cracks increases as the hydrogen concentrations increase, causing adjacent cracks to be connected. The crack generally initiates in the heat-affected zone in the C-Mn steel, but it could also propagate into the weld metal. These cracks are linked with the coarse-grained region and could be intergranular, transgranular, or a mixture. Five types of hydrogen-assisted impairment for metals and alloys are being considered by the ASM materials handbook; these are: (1)

hydrogen attack, (2) hydrogen-induced blistering, (3) hydride formation, (4) cracking from precipitation of internal hydrogen, and (5) hydrogen embrittlement [21]. Internal hydrogen embrittlement (IHE) is a part of hydrogen-assisted cracking (HIC), which is defined as the accretion of hydrogen, which already exists near large stress concentration sites and hydron environment embrittlement (HEE), elucidating cracking because of hydrogen sulfide or the exposure of hydrogen [22]. In the case of high-strength steels, hydrogen embrittlement is indeed a challenge, as the saline water along with other corrosive chemicals come into contact with it, which promotes the absorption of atomic hydrogen [23]. Several methods could be implemented to reduce the loss that occurs as a result of hydrogen cracking such as (1) minimum stress on joints, (2) proper preheating and post-weld heating, (3) appropriate selection of filler material, and (4) careful handle and storage of filler metals [24].

Another prominent issue in the pipeline industry is welding. Friction stir welding is a solid-state joining process invented at the welding institute in the United Kingdom. The friction stir welding was found to be efficient for joining hard to weld metals and joining plates of different thicknesses or different materials. The typical way to connect two natural pipes is shielded metal arc welding. When welding, we first need to tack the two pipes together to keep them in place. Then, we apply the method of butt welding. At present, to produce a flame hot enough to melt steel in the energy industry, this process involves the use of two gases: acetylene and oxygen. Through applying this flame to the steel being welded, a permanent weld is made; if required, an additional filler rod can also be attached to the welding area. Oxygen acetylene welding does not require the formation of electric welding. There are several disadvantages of this method, such as a visible hole being created in the welding plates. It is also less flexible as compared to the arc welding process. FSW cannot weld non-forgeable materials; also, filler joints cannot be created by it. Gas welding, on the other hand, showcases some advantages. This technique has the advantage of balancing the temperature at low temperatures. In the case of I-joint, it could weld the metal of thickness up to 6 mm. Generally, the pipes and tubes are welded in confined spaces, so gas welding is preferable here over other methods, as it requires equipment that is not bulky in nature. Moreover, this equipment does not require any electric supply. The light generated by its flame could be used to spot joints before welding begins. A major disadvantage of gas metal arc welding is the creation of a spatter, which are droplets of molten matter near the welding arc. It occurs when the welding currents are extremely high or in the case when gas shielding is not sufficient. For avoiding spatter, the welding current should be reduced, and the welder should correct the polarity. Moreover, a check over shielding gas type and flow rate should also be done [25]. Other common problems associated with gas welding include porosity, slag inclusions, incomplete penetration and fusion, incorrect wire delivery, deformation, cracks, and undercut.

2.1.1. Optical Endoscopy

Endoscopy: A boroscope and the use of CCTV are the means of visualizing the damage qualitatively. This image can be analyzed with advanced equipment to scan the contours in a topographic analysis and single out the defects. Laser ring triangulations and the visual odometry function with the deployment of crawlers mounted with equipment inside the pipeline is done [26,27].

Fiber Bragg Grating: These can be created using the property of variations of refractive indices of the core of an optical fiber, periodically. Utilizing predefined parameters, it is possible to predict the refractive indices at different places in the fiber with the variation of conditions of the environment. The light will result in constructive interference only at certain expected positions. There is a general relation for the wavelength variation [28,29].

$$\frac{\lambda_B}{\lambda} = (\alpha + \xi)\Delta T + (1 - \rho_e)\varepsilon \quad (1)$$

$$t = \frac{rP}{\sigma} = \frac{rP}{\varepsilon E} \quad (2)$$

where t = average wall thickness, r = average pipe radius, P = relative internal pressure, σ hoop stress, ε = longitudinal strain, ζ = thermo-optic coefficient, λ_B = Bragg wavelength, α = thermal expansion, T = temperature, ρ_e = photoelastic constant, and E = Young's modulus.

2.1.2. Electromagnetic Inspection

Inspecting through electromagnetic means would entail the utilization of fields after generating them. Electromagnetic health monitoring allows for the detection of burning, impact lamination, fiber breaking, and liquid ingress. The electromagnetic method essentially sends an electromagnetic image to the receiver to identify possible damage in the structure [30]. Their measurements and interactions yield the conductivity of the material and the test component's permeability. The different types of eddy currents generated, namely, Conventional Field, Remote Field, and Pulsed Field, provide the information as to the time or extent or decaying through measurements of the variation of these currents. Impedance is decreased with the permeability and conductance, and the phase lag is related to thickness of the wall.

$$\Phi_p \propto N_p I_p \sin(\omega t) \tag{3}$$

$$\Phi_e = \Phi_p - \Phi_s \tag{4}$$

$$d = 50\sqrt{\rho/f\mu_r} \tag{5}$$

$$\theta = x\sqrt{\pi f\mu\sigma} \tag{6}$$

where Φ_p = primary magnetic flux, N_p = number of primary coils, ω = frequency, Φ_e = equilibrium flux, Φ_s = secondary magnetic flux, d = depth, ρ = electrical resistivity, f = excitation frequency, μ_r = dimensionless relativity, θ = phase lag, x = distance between coils, μ = average permeability, and σ = electrical conductivity.

The above two relations define the measurement of the eddy currents.

2.1.3. Radiographic Inspection

The energy is directed through a source to a detector with a number of modifications performed on the rays that then produce a measurable damage quantity. The basic elements of all radiographic measurements remain the same. The radiographic method is particularly used in industry when isotropic material is encountered. They are not very precise and may even be damaging to the structure in certain cases, but they still are widely popular. The use of traditional X-radiography in the checking of carbon fiber/epoxy composites is limited, since they are low absorbers of X-rays. Thus, techniques that involve the use of penetrants (i.e., zinc iodide solution) have been introduced for enhancing the sensitivity of the method for these materials.

$$I = I_0 e^{-\mu x} \tag{7}$$

$$\mu = \frac{N\sigma\rho}{A} \tag{8}$$

$$\sigma = \sigma_{pe} + \sigma_s + \sigma_{pp} + \sigma_{pd} \tag{9}$$

$$E = I_f T \tag{10}$$

$$G_D = \frac{dD}{d(\log E)} \tag{11}$$

$$D = \log \frac{I_o}{I_t} \tag{12}$$

where I = intensity of a beam of radiation, I = radiation beam intensity entering the material, μ = linear attenuation co-efficient, x = material thickness, σ = total atomic attenuation co-efficient, N = Avogadro's constant, ρ = material density, A = atomic mass, σ_{pe} = photoelectric affect, σ_s = Compton scattering, σ_{pp} = pair production, σ_{pd} = photodisintegration,

E = film exposure, I_f = radiation intensity on the Film, T = time of exposure, G_D = contrast measured at density D , D = density, I_t = intensity observed on the film.

These techniques are applied in various ways.

Computed radiography involves digital scanning of the plates that are similar to the conventional films, and this allows reuse. Digital radiography nullifies the time lag between image production and ray penetration. This is tried in different orientations to produce different but predictable results.

2.1.4. Acoustic Method

Acoustic emission originally occurred naturally within materials, and the term AE is used to define the transient elastic waves that resulted from a sudden strain energy release within a material due to the occurrence of microstructural changes. When enough energy was released, audible sounds were produced. The cracking in timber subjected to loads near the yield point produces audible noises, which are indicators of impending failure of wooden structures, in the same way that the crying of tin, the cracking of rocks, and the breaking of bones are familiar to nearly everyone's ear. With a predefined threshold of noise, any extra generated vibrations that are produced by deformations of the pipelines will provide a location of the source of such a phenomenon. The magnitude of changes in frequency and intensity can be compared to different types and extents of the deformation and damage to the parts in question. Acoustic emission in the proper sense covers the audible frequencies up into the high ultrasonic range. Measurement today is carried out in the range between 50 kHz and 2 MHz. At higher frequencies, the acoustic emission is not intense enough in most cases, and the material absorbs large parts of the signal. In general, at lower frequencies, background noise disturbs the measurement e.g., vibrations from vehicles and noise from pumps or from flowing medium. Acoustic emission is especially used in places where leak size estimation is not as necessary as the accuracy [20,31,32].

2.1.5. Ultrasonic Technique

In the ultrasonic technique, we exploit the propagation of ultrasonic waves to obtain information about a mechanical component. For example, we can determine the mechanical properties of a material (the wave velocity is dependent on the material properties) or detect defects in a component (the presence of a defect will modify the characteristics of the propagating wave). Through combinations of various types of wave modes, coverage, transduction methods, transducer motions, and transducer configurations, a large number of possible configurations of detection of damage can be brought to light. The measurements of the voltages, time, and various other factors are listed in the following equations [31,33–36]. The main advantages of this technique are the low power consumption of the sensors and the capability to cover large areas using few sensors. The ultrasound technique for SHM consists of a system that is composed of several modules: signal generators that provide waves at specific amplitude and frequency with enough power to drive a series of sensors; several parallel acquisition systems for the signals received at the transducers; a digital control system to synchronize the modules, perform calculations on the signals, and determine the state of the structure; a communications system with a central node, which is critical when multiple structures are monitored; and, obviously, the piezoelectric transducers. All these modules must be embedded in a low volume system and show large capacities: high reliability, signal integrity, accuracy, speed of response, etc.

$$\rho \frac{\partial^2 u}{\partial t^2} = C^2 \frac{\partial^2 u}{\partial x^2} \quad (13)$$

$$C_1 = \sqrt{\frac{\lambda + 2\mu}{\rho}} = \sqrt{\frac{E(1 - \nu)}{(1 + \nu)(1 - 2\nu)\rho}} \quad (14)$$

$$C_t = \sqrt{\frac{\mu}{\rho}} = \sqrt{\frac{G}{\rho}} = \sqrt{\frac{E}{2(1 + \nu)\rho}} \quad (15)$$

$$C = C^0 - (dC/dT)\Delta T \quad (16)$$

$$\mu = Ae^{i(kx-\omega t)} \quad (17)$$

$$f = \omega/(2\pi) \quad (18)$$

$$\lambda = C/f = (2\pi C)/\omega \quad (19)$$

$$K = \omega/C \quad (20)$$

$$z = \rho C \quad (21)$$

$$R = \frac{Z_2 - Z_1}{Z_2 + Z_1} \quad (22)$$

$$d = \frac{Ct_r}{2} \quad (23)$$

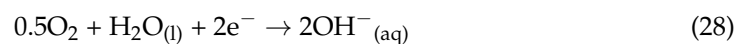
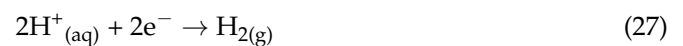
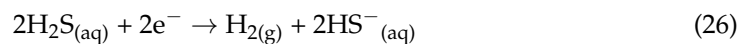
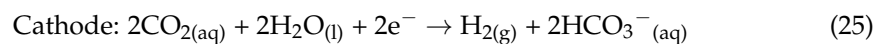
where u = velocity, t = time, x = displacement, ρ = mass density, C = speed of sound, C_1 = speed of sound for longitudinal, λ = Lamé's first parameters, μ = wavefront particle displacement, E = Young's modulus, V = Poisson's ratio, C_t = speed of sound for transverse, G = shear modulus, ΔT = temperature change, A = maximum particle displacement amplitude, ω = angular frequency, f = frequency, K = angular wave number, z = material acoustic impedance, R = reflection coefficient, Z_2 = transmission material acoustic impedance, Z_1 = incident material acoustic impedance, and t_r = total round trip time.

The waves that need the boundaries for their existence are known as guided waves. When the longitudinal and shear bulk waves undergo constructive interference, ultrasonic guided waves are generated. There are several advantages of using ultrasonic guided waves in structural health monitoring, which include (1) long-range inspection, (2) full exposure of waveguide cross-section, and (3) high sensitivity to small defects compared to overall vibrations [37]. Due to their capability of inspecting large formations from a single probe position, ultrasonic guided waves are considered a great tool for structural health monitoring. Furthermore, it also possesses excellent flaw detection, and it could also establish wave resonance by tuning its frequency and setting up its mode. Different methods comprising magnetostrictive-type sensors, angle beam transducers, and comb-type transducers can be utilized to produce ultrasonic guided waves in a structure. The advantage of ultrasonic guided waves includes their assessment ability of concealed structures—which are present underwater as well as in concrete, coatings, and insulations—with magnificent sensitivity. Due to its simplicity and speed, it is considered a cost-effective solution for structural health monitoring [38]. The application of ultrasonic guided waves includes various structures such as tear straps, landing gears, lap splice joints, and so on. Its aircraft applications are also presented in the references [38–42]. Ultrasonic guided waves can also be used to perform surgery by the harmonic scalpel. In this case, the energy used for activation is sent to the tip of the rod, which is deployed for surgical use [43]. These waves are also used in inspecting rails in the railroad industry [44–46]. Moreover, guided waves could also show their impact in some adhesive bonding and joining applications [47–49]. At the interface between materials, these waves can generate both longitudinal and shear waves energy, which is especially useful in the adhesive bond inspection. The result of the dispersion of a sample guided wave is illustrated in Figure 5. Fourier transform was applied to obtain this profile, and then, the result obtained is compared with the theoretical value in which the dominant modes of the structure are highlighted [50].

3. Health Monitoring in Corrosion

The estimated corrosion-related cost is about \$5.8 billion annually to monitor, replace, and maintain these assets. It has been estimated that corrosion costs a sum of \$1.4 billion annually to the United States in production and exploration alone, with \$589 million used in surface pipeline and facility costs, \$463 million in downhole tubing expenses, and \$320 million in capital expenditures related to corrosion [51]. One out of every four natural

gas transmissions and gathering incidents has been the consequence of corrosion in the last three decades according to the Pipeline and Hazardous Materials (PHMSA) database, and more than half of these were due to internal corrosion [52,53]. However, it is even more difficult to inspect the insides of a pipe, and more so when the pipe is thousands of kilometers long and the problem could be anywhere. Hence, steps have been taken to achieve easier detection in these scenarios. Corrosion is an electrochemical process and usually requires an anode, a cathode, and an electrolyte to occur. These components are fulfilled by the fluids found in the reservoirs, thereby promoting corrosion [54–59].



This reaction causes a decrement in mass and material and also unexpected cracking and catastrophic failures in oil and gas industries. Corrosion is thermodynamically favorable, so it occurs, but its kinetics can be brought under control. Localized corrosion or pitting occurs due to hydrogen sulfide and chloride ions, which provide structural weak points, resulting in cracking without the force being enough to cross the mechanical threshold. Microbes are also another causative agent of corrosion, especially the sulfate-reducing ones [60–62]. More than one-quarter of the damages done by corrosion could have been prevented in the United States. Widely used carbon steel is prone to corrosion; monitoring it to plan maintenance can be helpful in corrosion prevention [51]. The carbon steel is used in many places including drill pipes, transmission pipes, and casing tubing [63] owing to its excellent mechanical properties and reasonable prices. SHM is required to detect signs of risk that could cause catastrophic events. Monitoring allows for the identification of corrosive elements, and this especially comes in handy when thousands of miles of pipes are being discussed. Corrosion sensors are broadly classified as direct or indirect based on detection through environments or consequences. The optimum type of sensors needs to be selected in this scenario (Figure 1).

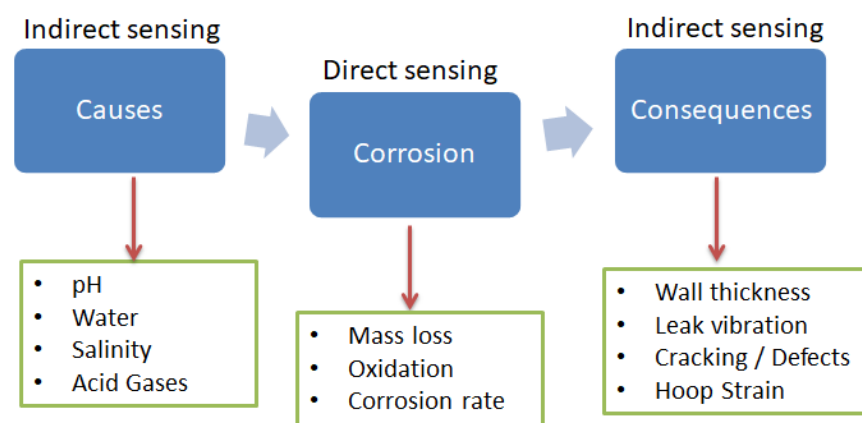


Figure 1. Categories of corrosion sensors and their characteristics with the causes and consequences.

3.1. Conventional Corrosion Sensors

Conventional and commonly used corrosion sensors for SHM techniques in the O&G industry are discussed in this section. A review or summary on corrosion monitoring techniques in general or other areas is also available in references [64–67].

3.1.1. Corrosion

A corrosion coupon involves placing a certain patch of a material for a certain corrosive environment. The coupon is designed to be able to satisfy our needs to realize the rates of corrosion. It has a known weight and shape. The weight it loses is measured to find out the actual damage done by corrosion [68]. This type of technique is unable to give an analysis of corrosion when it actually happens and just gives a mean rate of the corrosion that would take place. The coupon is normally placed within the working material, and hence, another one of its drawbacks includes the fact that it is difficult to remove and then to be placed again (Figure 2). Its versatility lies in the fact that any shape or weight can be used to find out the corrosion rate.

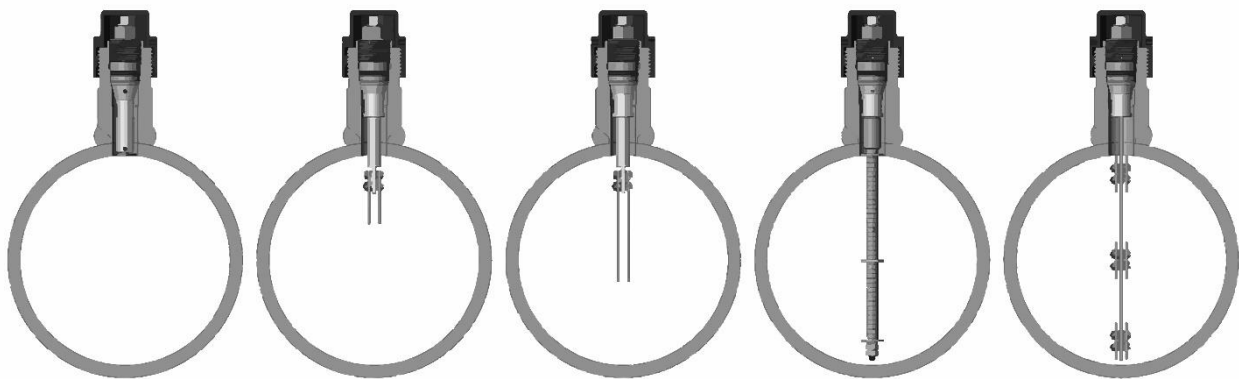


Figure 2. The different types of corrosion coupons installed inside the structure.

3.1.2. Electrical Resistance Probe

Owing to corrosion, there is a reduction in the material's mass, and this fact can be advantageous, since the resistance is increased due to a lowered material mass, and this resistance can be measured to get to the proportional relationship between mass loss and resistance in the material. Since resistance has the ability to fathom the amount of corrosion in the material, it can be termed as a real-time corrosion coupon. With the help of this technique, it is possible to remotely log in data. Since it is possible for them to operate in conducting and non-conducting surroundings, it can be considered to be an additional advantage. Water-based corrosion is responsible for a conducting environment, while atmospheric corrosion is responsible for non-conducting. Electrical resistance-based investigations are plagued with primarily one disadvantage, which is that they are not equipped to identify variable corrosion, which means that if the amount of corrosion occurring at various places is not uniform, then an electrical resistance probe will give a result that is averaged throughout. If there is a requirement for an increased sensitivity toward variable corrosion, then multiple probes will have to be installed, and thus, it would complicate the system and increase the monetary investment needed.

3.1.3. Electrochemical Sensors

The electrochemical characteristics of corrosion are elevated with the help of electrochemical sensors, which make use of techniques such as galvanic current measurement, linear polarization resistance (LPR), electrochemical impedance spectroscopy (EIS), and electrochemical noise (EN) [10,67,69–71]. Electrochemical sensors are fairly advantageous; they can include the measured corrosion rates, and they also have the ability to investigate the mechanism responsible for the resultant corrosion. There are a myriad of electrochem-

ical techniques, but the LPR-based corrosion technique has been used as a commercial method, since it is simple to operate, and the interpretation of data here is easier as compared to other methods. In most LPR-based investigations (Figure 3) [72], the traditional concept of having a three-electrode system is not followed. Rather, the electrodes are made from the same material. In the case of electrochemical sensors, the disadvantage lies in the fact that because of external potential, the corrosion rates can go up. Thus, in order to avoid this, it is necessary that parameters such as overpotential, scan rate, and Tafel slopes are chosen with accuracy. There is an additional requirement of an electrolyte that is ionically conducting, making them unfriendly for usage in a non-conductive environment. There is an electrochemical corrosion sensor that can operate even at a temperature of 300 °C and at a pressure of 5000 psi. This sensor makes use of the galvanic current in a coupled multi-electrode array [73,74] (Figure 3) [75] to detect the localized corrosion. With the help of an Advanced Electrochemical Sensor (AES), the amount of water and the rate of corrosion in simulated natural gas were measured (Figure 3) [76,77].



Figure 3. Variations of the electrochemical sensors. Reproduced with permission from [77] Copyright 2019 AIP Publishing.

3.1.4. Ultrasonic Testing Sensor

One of the most common methods that monitors the extent of corrosion and the structural health of the pipes is the method where ultrasonic testing (UT) wall thickness is measured. Acoustic waves that have a high frequency, of the order of MHz, are generated from a piezoelectric transducer. The direction in which these waves are emitted is in a direction perpendicular to the pipe wall. The transducer receives the waves, which are reflected from various surfaces such as the internal and external surface of the pipe. The wall thickness is calculated by measuring the time difference between two consecutive echoes from the outer and inner surfaces of the pipe [78–80]. The data of wall thickness and stand-off signal are combined together to understand the difference between internal and external material losses in the pipe, as shown in Figure 4 [32,81]. The UT sensors are available in fixed as well as portable forms [71]. In addition, they can be added together with in-line inspection devices. This method has the capability to inspect corrosion by accessing only one side of the pipe. Highly attenuating mud and casing scales affect the acoustic sensors in the most direct fashion [3].

3.1.5. Magnetic Flux Leakage Method

This is yet another marvelous method that does not severely damage the system for monitoring; instead, it uses the magnetic properties of the substance. It can detect a change in flux. The flux changes simply because the flux line always exist in ferromagnetic substances. Normally, the undeformed structures will have a simple continuous and will produce magnetic lines in a fixed direction. However, when a defect is encountered, it surely would have caused some misalignment of the magnetic flux lines due to the deformation. This magnetic field change can be used to interpret a variety of information about the damage (Figure 5). The only problem that it faces is the differentiation in location of the damage and the inability of the confirmation of a reason for the damage. In addition, it can only detect damage; it cannot predict it [82,83].

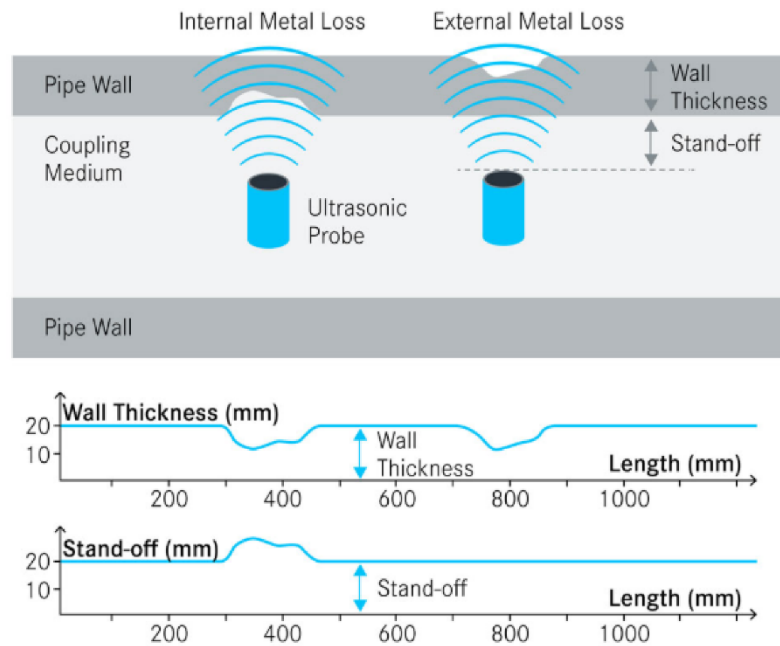


Figure 4. Ultrasonic texting that can discriminate between internal and external mass loss.

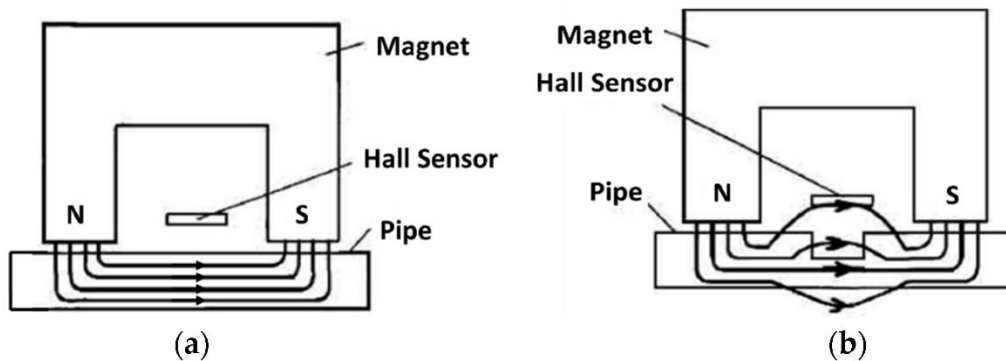


Figure 5. The principal of a magnetic flux leak sensor that can measure the flux passing through and interpret it to give meaningful results [83]. (a) A ferromagnetic material only has all the lines inside it. (b) Hall-effect sensor.

3.2. Point OFS for Corrosion

It can be considered that point corrosion OFS is an optical version of corrosion coupons. At a particular section of optical fibers, the point OFS generally consists of coated sensing layers. Generally, the optical fibers are metallic films. It can be seen in Figure 6 that as there is corrosion of the metallic films at the ends of the fiber, there is a reduction in the reflected light, and at the other end of the fiber, this light is detected [84,85]. On the other hand, there is a coat of Fe-C film over a particular section of the fiber, and accordingly, there is an increment in the transmission of light along the optical fiber as the corrosion of Fe increases [86]. The long-period grating (LPG) is an alternative method to design a point sensor that allows the interaction of light and the neighboring medium with the help of cladding modes. The periodicity of LPG (Λ) ranges from 100 to 1000 μm , and this is greater than the periodicity range of fiber Bragg grating (FBG), and light from the guided mode is coupled into the core, which then moves toward the forward propagating cladding modes at particular values of wavelengths. Due to this, there is an evident dip in the transmission spectrum, as can be seen in Figure 7. Resonant wavelengths show strong changes toward even smaller changes in the temperature and strain of the cladding modes [87,88]. In a comparison between FBG and LPG, it is found that LPG exhibits higher

magnitudes of spectral shifts and thus, owing to the larger values of periodicity, fabrication becomes simpler [87]. Various studies have been carried out that are focused on LPG sensors consisting of an Fe-C coat, and the studies have been carried out to observe the loss of mass due to corrosion [89,90].

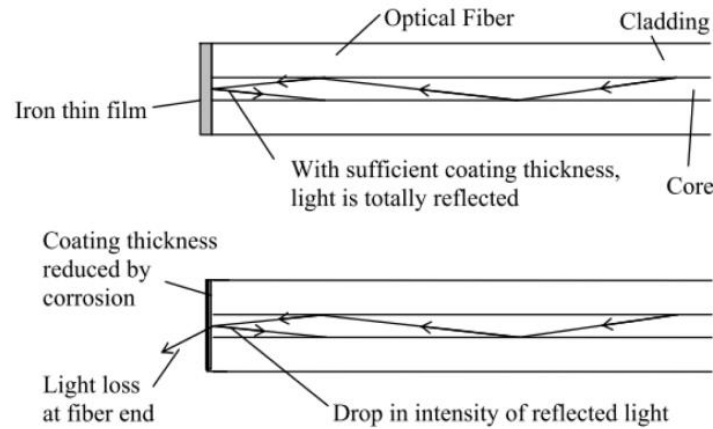


Figure 6. Change in intensity of light results in the detection of corrosion [85].

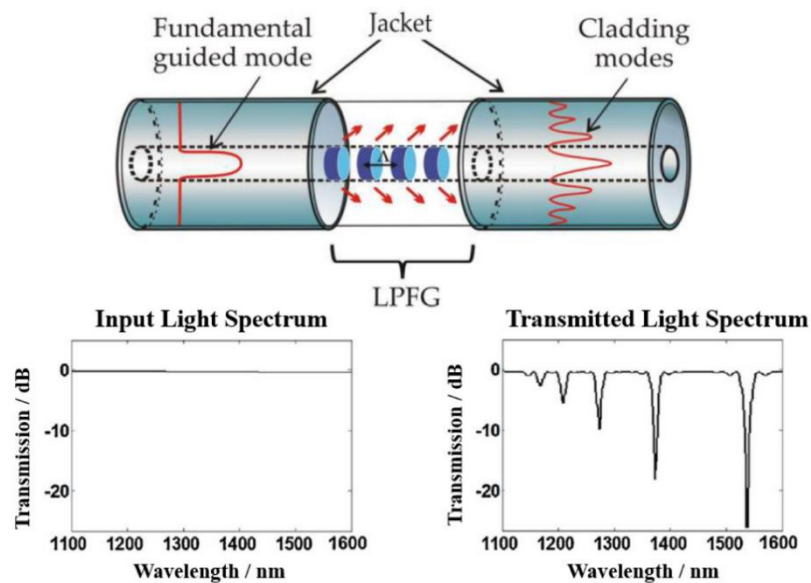


Figure 7. Light spectrum data indicating presence of anomalies [71].

3.3. Quasi-Distributed OFS for Corrosion

It can be considered that sensors based on Fiber Bragg grating are equivalent to point sensors. For every FBG sensor, there is a shift in the Bragg wavelength owing to the changes in the environment such as changing temperature and strain. On the basis of this principle, it becomes possible for the FBG sensors to be able to monitor the changes in temperature and strain parameters which are closely related to the corrosion that happens in pipelines and wellbores (Figure 8).

$$\lambda_B = 2 n_{\text{eff}} \Lambda \quad (29)$$

The FBG-based pressure sensors that have been developed can be utilized in finding the point of leakage in the pipelines by using the method of negative pressure wave (NPW). When a leak in a pipeline initially happens, there is a pressure drop that is induced, and it travels in either direction from the point of leakage. The NPW reaches the FBG pressure sensors that are fixed on the pipe, which records the time taken for the wave to reach it,

and this information is utilized to evaluate the point of leakage [91,92]. It has been found that the strain sensors based on FBG are attached directly to the pipeline surface in order to evaluate the strain of the refurbished pipes [93]. In field tests, the installation of sensors based on FBG are done over the risers for watching the riser stress during drilling-based operations such as subsea drilling (Figure 9b) [94–96]. When a coat of hygroscopic polymers is done over the FBG-based structures, these structures can then be utilized as an H sensor, since there is a mechanical expansion that happens inside the polymeric structure [97–99].

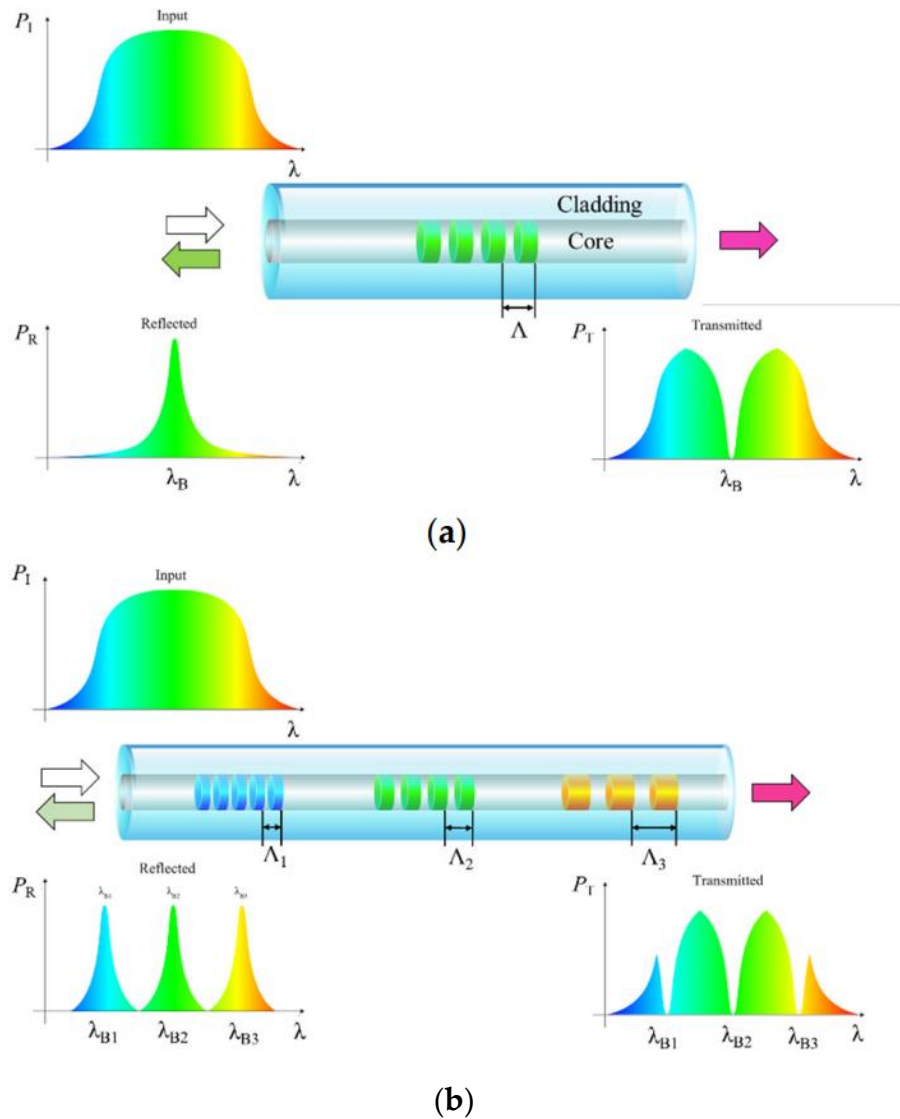


Figure 8. Optical spectral responses of (a) single and (b) multiple fiber gratings [71].

3.4. Distributed OFS for Physical Sensing

Brillouin scattering is a kind of an inelastic scattering that happens due to acoustic waves generated by the lattice vibrations. This kind of scattering is also extremely sensitive to the temperature and deformation value of the optical fiber. Another kind of inelastic scattering is the Raman scattering, which happens due to the exchange of energy with the molecular vibrations of the fiber. Technologies such as distributed temperature (DTS), distributed strain (DSS), etc. have grown massively in previous decades [100], and thus, their adaptation for monitoring the corrosion and structural health has been carried out in the oil and gas industry. Apart from monitoring the temperature, strain, etc. during operations such as well logging [101], the utilization of distributed OFS has been done in

order to monitor various physical parameters that are associated with corrosion, failure, and leak detection.

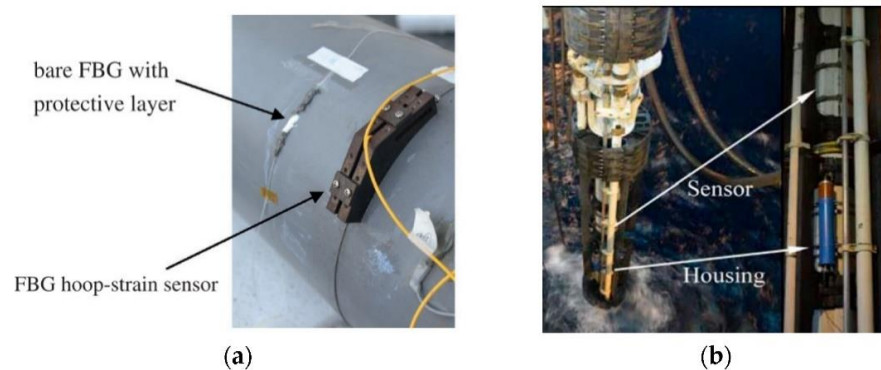


Figure 9. (a) Photograph of FBG hoop strain sensors that are wrapped around a pipe. (b) Field demonstration of the sensors based on FBG that monitor the riser stress for subsea drilling and operations [71].

The thermal properties of the fluids flowing inside a pipeline are the ones to detect any kind of leakage in the pipeline, and DTS is largely used for this purpose. One of the methods to lower the viscosity of the flowing fluids, such as crude oil, is heating transportation for a more efficient flow of the crude in the pipes. Any leakage of these hot oils would lead to a considerable amount of temperature change on the outer surface of the pipelines, which is easily detectable with the help of DTS [102]. It can be explained from the Joule–Thomson effect that when a gas exhibiting higher values of pressure leaks, there is a reduction in the resultant temperature. The leakage of liquids leads to an increment in the temperature due to which the DTS detects a leakage in the pipelines [101].

The DAS that makes use of coherent Rayleigh backscattering was studied to see if they are capable of detecting vibrations in a pipeline that are induced due to leakage. The investigation was carried out with the help of optical fibers, which are wound over the pipes in a helical fashion (Figure 10) [103,104].

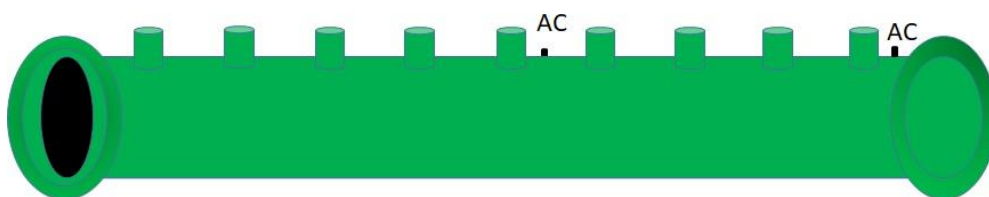


Figure 10. The wires are helically wrapped over a pipe of this type to result in the ability to measure acoustically the health of the system [87].

3.5. Distributed OFS for Chemical Sensing

Using sensors outside the pipelines to identify and evaluate the early signs of corrosion after it has occurred and once the structural integrity has worsened is the most appropriate method. A less advanced version of sensors when compared to DTS, DSS, and DAS are DCS (distributed chemical sensing), which demonstrates a remarkable capability by tracking corrosive conditions to promote corrosion prevention before or at the initial diagnosis of corrosion. The feasibility of sensors made up of optical fibers is achieved by activating the operational chemical coating (polymers, metal–organic frameworks, nano-materials, metal–oxide films, etc.) over their core or cladding. To enable the association of light with these chemically sensible layers over the core or cladding and with the external medium [105–107], the optical fibers may be carved, trimmed, stitched, or edge-polished.

Since its emergence in the 1990s, a special class of fiber structure for OFS with tremendous capability for DCS has been provided by micro-structured optical fibers [108–110], which features the air holes extending along the whole length of the fiber parallel to the longitudinal axis known as photonic crystal fibers (PCF) [108–111], unless the air holes are regularly organized within the cladding matrix. Figure 11 shows the internal and external look of an evanescent field-based semiconductor [112].

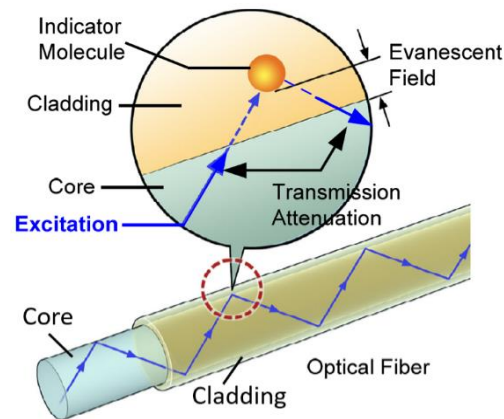


Figure 11. The figure shows the internal and external look of an evanescent field-based semiconductor Reprinted with permission from [112] Copyright 2014 Elsevier.

While microstructured fibers provide highly sensitive and versatile fiber structures, large production and marketing are still limited, demanding the cost-effective long-distance production of such fibers. By the direct association of light with gas in holes, few PCF sensors (index guided and hollow-core) were observed to track highly sensitive gases such as methane, hydrogen sulfide, carbon dioxide, and acetylene (ppm level) [113–117]. Specific detection for Cl and humidity control with a Cl^- sensitive material that shows fluorescent behavior filled in the gaps; a suspended-core fiber PCF sensor has been developed [118]. The use of proxy materials incorporated with the dispersed OFS network to specifically track corrosion as a decentralized optical coupon and provide information about them is a new idea for corrosion diagnosis, which is planned to be mounted along the inner surface of the pipelines to control internal corrosion. For decentralized corrosion control, while examined using OFDR, metallic film-coated optical fibers have been presented where the loss of mass is tracked on the basis of the change in intensity or change in strain along with the optical fiber [71,119,120] (Figure 12). In the corroded area, the light intensity and the strain increase due to the release of compressive internal stress followed by electrodeless deposition of Ni film as the light absorption of the metallic film reduces and the film becomes thinner. Decentralized monitoring of important environmental variables such as quality of water, the conductivity of the electrolyte, and acidic gases (carbon dioxide and hydrogen sulfide) will assess the corrosivity of the atmosphere and thus track corrosion indirectly. While only a few research studies have examined DCS [119,121–123], chemical sensing materials are being studied for a wider variety of optical fiber applications, which could theoretically be used for the production of DCS to track corrosive external factors. For compatibility with OFS, there are a number of pH-sensing materials, including localized surface plasmon resonance (LSPR) Au or Ag nanoparticles (NP) integrated composites (Figure 13a) [124–126], organic dyes [127–132], fluorescent molecules [133–137], polymers [138–141], pH-sensitive hydrogel [142–145], etc. The pH value of the solution independent of the material embedded in the matrix is observed to be more integrated with the silica matrix coating [124,146]. For more information regarding the sensitive pH products and optical fiber pH sensors (Figure 14), refer to these references [145,147,148]. To measure the emergence of water, ion intensity, and temperature, graphene oxide coatings and polymers have been tested, and at the same time, with no covering by measuring phase transition in all ways (Figure 13b), a multi-sensor OFS has been designed that can

also help in monitoring the internal corrosion within natural gas pipelines [107]. In the case of acid gas detection, salinity tracking, gas-sensitive coatings, or gas absorption sheets are also used in OFS, which are based on the changes in the refractive index using tapered optical fibers [118,149–151]. MOFs that can absorb CO₂ have shown rapid, reversible, and promising results for monitoring CO₂. Along with the employment of pH, indicators are a must in case of CO₂ monitoring, as it can reduce solution pH value. Some examples of OFS chemical sensing layers for corrosivity control are mentioned in Table 2.

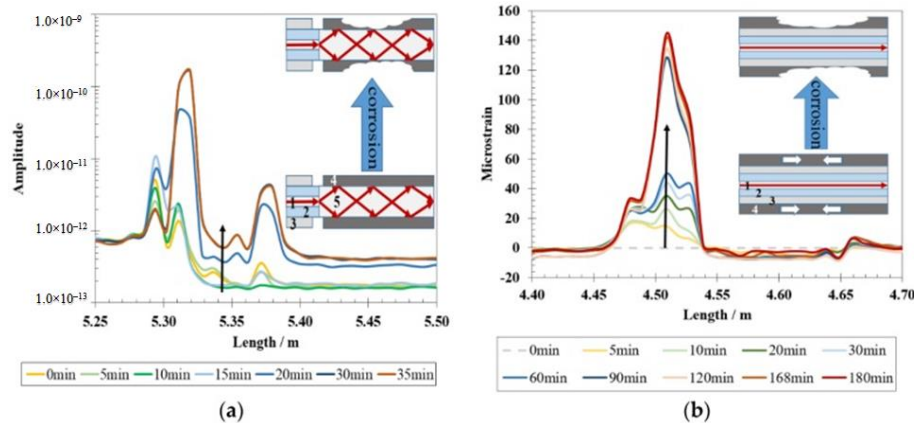


Figure 12. Metallic thin film-coated optical fiber sensors (OFS) for distributed corrosion sensing interrogated using Optical Frequency-Domain Reflectometry (OFDR) [71]: (a) Rayleigh backscattered light increases as the corrosion of Fe proceeds due to light absorption of metallic film; (b) Microstrain on the fiber increases with mass loss of coated Ni film due to release of compressive internal stress induced by Ni deposition. Note: (1)—single-mode fiber core; (2)—cladding; (3)—polymer jacket; (4)—coated metallic film; (5)—multi-mode fiber core.

Table 2. Techniques of SHM and their descriptions.

SI No	Name of SHM Technique	Nature of Technique	Applicable Infrastructure	Precision of Damage Detection	Use for Water-Based or Oil-Based Conduit	Potential to Predict Future Damages
1	Corrosion Coupon	Coupon is placed within the working material and is thus invasive	Can be applicable for pipe/reactor of any shape or size	No precision position and time of leak/corrosion	Can work for water-based system	Difficult to predict any future damage location
2	Electrical Resistance Probe	Invasive probe works as a real-time corrosion coupon	Can be applicable for pipe/reactor of any shape or size	No precise positioning but time and extent of corrosion or mass loss can be determined	Can work for oil or water-based system	Real-time data may be utilized to detect the future damage or probable future leaks
3	Electrochemical Sensors	In-situ electrochemical corrosion rate determination	Can be applicable for pipe/reactor of any shape or size	No precise positioning but time and extent of corrosion can be determined	Work better for ion-conducting electrolytes. Externally imposed potential may increase electrochemical corrosion rate	Difficult to predict any future damage location
4	Ultrasonic (Acoustic) Testing Sensor	Ultrasonic probes are placed inside the pipe to detect pipe thickness, flow change, or loss	Can be applicable for pipe/reactor of any shape or size	Precision is better than corrosion coupon or other corrosion sensors. Real-time positioning is possible. However, very small leak or structural damages are difficult to determine using this technique	Can work for oil or water-based system	Real-time data may be utilized to detect the future damage or probable location of leaks in future
5	Magnetic Flux Leakage Method	Invasive technique for detection of damage in structure by comparing magnetic flux lines	Can be applicable for pipe of any shape or size	Cannot precisely locate the position of structural damage	Can work for oil or water-based system	Using this technique, it becomes difficult to predict any future damage location
6	Point OFS for Corrosion	Works as an optical corrosion coupon using optical spectrum from its position inside the pipe	Can be applicable for pipe of any shape or size	No precise positioning but incidence and extent of corrosion can be determined	Can work for oil or water-based system to determine structural damage	Difficult to predict any future damage location

Table 2. Cont.

Sl No	Name of SHM Technique	Nature of Technique	Applicable Infrastructure	Precision of Damage Detection	Use for Water-Based or Oil-Based Conduit	Potential to Predict Future Damages
7	Quasi-Distributed OFS for Corrosion	It uses FBG-based external point sensors to determine change in temperature and strain. The pressure wave generated transmits both the directions from point of leakage, where the pressure sensors detect the leakage point by analyzing the pressure wave	Very useful to determine the corrosion in pipeline and wellbore in real time	Precise point and time of leakage can be determined using this technique of negative pressure wave (NPW)	Can work for oil or water-based system to determine structural damage. It can detect gas leaks	Can be useful for predicting future leaks or damage
8	Distributed OFS for Physical Sensing	Parameters of corrosion and leaks are determined by monitoring pressure and temperature change due to leaks. Optical fibers are wound over the pipe to detect the leak	Determination of corrosion and structural change in well. The technique is also useful for determination of efficient flow of crude in pipes and impacts in flow due to corrosion	The leak can be determined precisely and in real time	Can work for conduits carrying oil, waters, and gas	The technology can be extended to determine corrosion or damages in pipe
9	Distributed OFS for Chemical Sensing	Optical fibers with chemical coating and air holes are activated over the pipe core or cladding. Can be applied to check the external or internal health of a pipeline structure	Multi-sensors OFS are designed and utilized to determine leaks of gases of different types and the nature of environments the conduits are exposed to.	Precise determination of leaks and damages are possible in real time	Can work for conduits carrying oil, waters, and gas for leak detection	It gives early signs of corrosion. It is the best method to predict damage or leaks
10	SCADA and CMS	Acoustic emission, optic fiber, thermographic, photogrammetric techniques, and others are used to remotely collect and monitor the external conditions of infrastructure frequently via SCADA and CMS. Then, the data are communicated to determine damages in infrastructures	Determine the damages in external parts of wind farms. The techniques can also be used to detect damages in pipelines and other infrastructures	External damages to infrastructure can be monitored. General cracks can be determined. However, very fine leaks may not be detected in real time.	Can work for conduits carrying oil, waters, and gas	Monitoring external conditions may not always indicate any impending danger
11	UAV-Based Technique	Multi-sensor (thermal, laser, sonic, spectroscopic, photogrammetric) remote sensing of crack and structural deformations using UAV platform	Determine the external damages to any infrastructure of the oil and gas industry	Laser UAV can detect fine damages if scanning is done from close proximity. Data are required to be analyzed to determine the leaks. However, it would need the help of ground-based/internal sensors to know about any leak and then can fly over the damaged part to make detailed monitoring of damaged infrastructure	Can work over oil, water, gas conduits, or any other infrastructure	The damages existing at the pipeline or infrastructure may be extrapolated to determine the future source of leak or gas emissions. However, prediction requires inputs from other accurate invasive techniques to comprehensively monitor the existing situation and any likely situation that can develop in the future
12	Ground Penetration Radar Sensing	Underground sensing technique by GPR instruments	For underground civil structure oil and gas pipelines	Use electromagnetic waves that are transmitted through an antenna moving along the surface to the monitoring object	Underground pipeline leak detection	Reliable and leak information is comprehensive when leaks are found in underground pipelines
13	Analysis of the Pressure Point	Monitor pressure difference in pipeline by contact and non-contact sensors	For dill bits and oil and gas pipelines	The pipeline system controls pressure variations at various points	Cold climates and working properly under various flow conditions	Suitable for submarine environments

Table 2. Cont.

SI No	Name of SHM Technique	Nature of Technique	Applicable Infrastructure	Precision of Damage Detection	Use for Water-Based or Oil-Based Conduit	Potential to Predict Future Damages
14	Infrared Thermography	Remote sensing of cracks and by thermal photogrammetric camera	For tall structures and oil drill bits	Easy to use and fast response time for converting detected objects into visual images	Detection of pipeline temperature variations	Detect leaks with infrared picture techniques to detect pipeline temperature changes
15	LiDAR Sensing	LIDAR sensing for small cracks by LiDAR scanner	For oil and gas pipelines as well as minor cracks detection for civil infrastructures	In the absence of any temperature variation between the gas and the environment, the leaks can be detected	The pulsed laser is used for methane detection as a lighting source for pipelines	Methane detection light source for gas pipelines

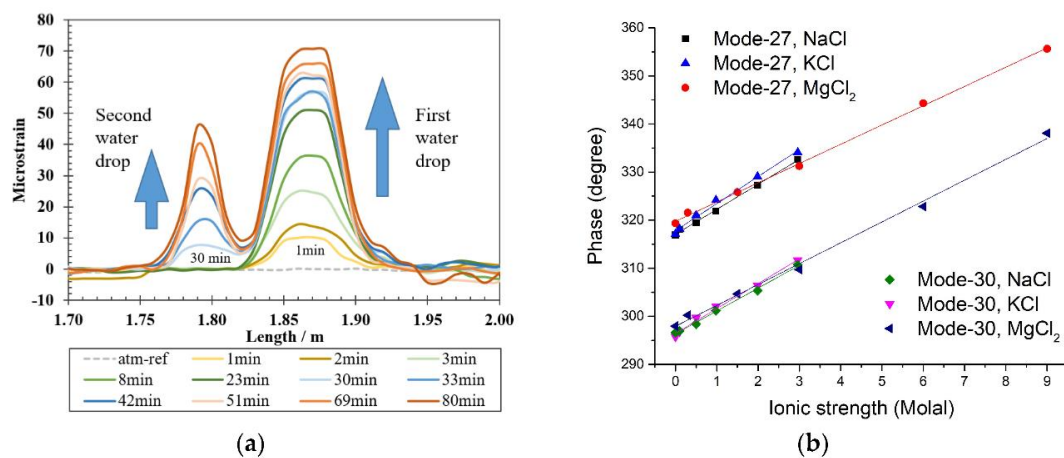


Figure 13. (a) Demonstration of distributed water detection in air based on the swelling-induced strain changes interrogated with an optical backscatter reflectometer (OBR). The first water drop was added at 1 min, and the second water drop was added at 30 min [71]; (b) Phase shift-based optical fiber sensor (OFS) without any additional coating for simultaneous multi-parameter monitoring including ionic strength as a corrosivity indicator [71].

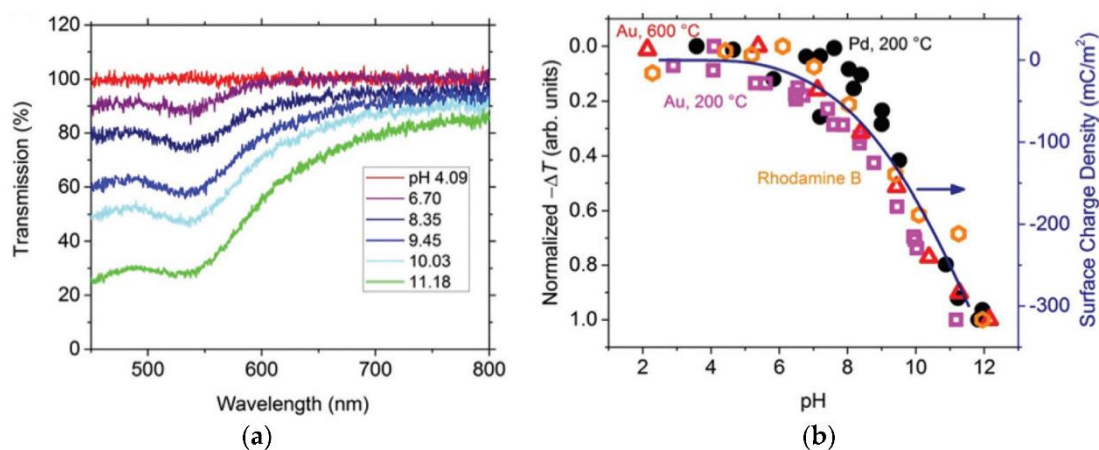


Figure 14. (a) Transmission spectra of optical fiber pH sensor coated with localized surface plasmon resonance (LSPR) Au-nanoparticles-incorporated SiO₂ layer at different pH; and (b) pH sensing results from silica matrix coatings embedded with a variety of optically active materials. Reproduced with permission from [124] Copyright 2014 The Royal Society of Chemistry.

3.6. Challenges of OFS Application in the O&G Industry

The extreme conditions that can be found in the oil and gas well bore pose a certain difficulty in the monitoring of the downhole. This occurs by the presence of carbon dioxide, hydrogen, and mechanical stresses. The OFS can be relied upon for downhole sensing but with temperatures as high as 300 °C and hydrogen ingress, the silica fibers are dangerously affected. The presence of water can be instrumental in this also, resulting in long-term instability [101]. The silica hydrogen bond with adsorption of hydroxyl can result in extrinsic attenuation. As a counter-action to this, a hermetic carbon layer can be added for protection of the silica, but this idea would also fail at the unusually high temperatures encountered, resulting in an increased importance of protective coatings [152,153]. The alternatives for silica include sapphire cladding, which is highly expensive. If the cost can be overlooked, it normally eliminates the problem and can still work at 1800 degrees. Another challenge is the transfer across long distances and across the hundreds of thousands of miles of pipeline infrastructure with high resolution. There is a common compromise between high-distance transmission and the resolution received. OFS aims to decrease this problem and lead to an optimized system [104,154–162].

4. Health Monitoring Techniques for Wind Farms

4.1. Supervisory Control and Data Acquisition (SCADA) and Content Management Systems (CMSs) for Health Monitoring

SCADA and CMSs are the two most recognized health monitoring systems and come very handy when offshore wind farms are considered. Being too distant from the mainland, these wind farms require constant monitoring. They monitor the elementary components and also take care of the difference in input factors including the [163] wind speed and outputs. It is ensured that the sampling frequency can be managed at 0.02 Hz at an interval of 10 min for monitoring. This small interval allows for analysis before it is too late to find the error that has occurred and the details such as the extent and location where it has happened. The program also provides real-time solutions or suggestions. Researchers also find the log data to be very useful in their work, which in turn creates an environment for the creation of even better systems of monitoring. Further studies provided an insight into the combination of different systems and SCADA monitoring to present even reliable combined machines. Notable are the uses of the neuro fuzzy system [164,165], Bayesian frameworks [166], and Yang's varying conditions [167]. Another important tool in the same line is the CMS, which has the capability to identify damages through vibrations at higher frequencies, normally 50 Hz or higher, and the response system collects data at an even increased frequency [168–170]. CMSWind and the ADAPT.wind system are the newer and modified forms of the traditional monitoring systems. The only logical next step was to combine these two major systems, SCADA and CMS, together. It is a huge task but could combine the best features of the two. Examples of this combination/integration are the Intrusion Detection System (IDS) and Wait Time Information System (WTIS) systems. A combined basic setup is depicted in Figure 15 below.

4.2. Health Monitoring System of Blades

The most important part of the wind energy generation and also the ones that can be most easily affected by damages are the blades of a wind turbine. They are made up of a wide range of elements that are combined together. They also need to maintain high flexibility, and thus, any damage that they face gets easily transmitted to the whole blade, causing them to wear easily. The damage spreads as cracks and delamination. The damage can be harmful because it can cause imbalance, which will not only disrupt the readings in general but also cause major catastrophic events leading to destruction of the wind farm.



Figure 15. SCADA and CMS systems common description and specifications of use.

These are the reasons that make the monitoring of the damage of the blades so important. The first stage is to find out the way for perfect monitoring, which would include testing and analysis. Sutherland in 1994 analyzed the blade with non-destructive techniques: acoustic emission and the coherent optical technique. The technique for blade analysis continued including neural network systems and wireless sensor networks [171–173].

One of the major problems in creating monitoring systems for a blade is the dynamic conditions faced by blades. Static systems can in no way emulate the ever-changing conditions a blade has to face. It almost makes it necessary to have a monitoring system for the monitoring system itself. The wind harvester is an acoustic emission-based telemetric system, e.g., NEG-MICON NM 48/750, which can collect data for about half a year [174–176].

Furthermore, the wind turbine changes a lot of its properties when it faces damage, and thus, the damage receptor and interpreter will also have to be very adaptive while looking at the damage and thus inherently change the parameters for reading the damage as the damage increases. Based on this observation, a system to adapt to changes was introduced known as the SMART Wind Turbine Rotor project, which integrated a number of condition-analyzing tools that could provide real-time analysis on the blade conditions; it was developed by the Sandia National Laboratory [177]. An even better version known as the fibrous Bragg grating sensor attracted attention due to being unaffected by the electromagnetic radiations and thunder; it also was more durable and required lesser maintenance [178]. Modified forms of the above ideas integrated into different materials and locations were utilized for better and more accurate results.

Thermal and electromagnetic technologies are also not lagging behind when it comes to monitoring. Apart from the mechanical methods, Ozbek has made use of strain gauges, photogrammetry, and laser interferometry to identify the blades according to several conditions tested at different speeds [179]. A laser thermographic system also became popular in being able to analyze the damage and simulate it in a different place [180,181].

4.3. Health Monitoring System of the Tower and Foundation

The problems and threats that the support pillars of the wind turbine face are pretty different from the ones that the blades face. The major reason is that the pillar has to bear a specific weight on the same place for a long time. It has to be robust to continue to carry the maximum weight without faltering, because even though its monitoring may

require a different method, its safety is as important as that of the blade. If there is even a small imbalance in the support or a change in its stress-bearing capacity, it could lead to a serious flaw in the calculations and subsequently the wind energy productions. In addition, monitoring of the blades will be affected by a fault in the support.

The wind turbines that are used in off-shore applications were developed much later, and due to that reason, their monitoring systems are much more effective. This is because with older projects, the structural designs and aerodynamic properties could not be optimized to fit in a proper monitoring system. However, due to being built later with the idea of the advanced monitoring system already in the works, their design is good and accommodating. The SCADA system has been utilized, but it is not very effective when it comes to a decreased sampling frequency [182,183].

For overcoming this problem, the wireless network sensors were utilized that had the range of 50 to 150 Hz in three intervals for sampling purposes, which allowed total offline modal analysis of the towers. The SESHMS is a comparatively more economical system that was released as a further development. They have established small programmable Object-Oriented Technology using software to wirelessly transfer data to neighboring receiver nodes. It smartly used the DSL system for the study of dynamic data of displacement, temperature, acceleration, and wind speed during the same time period for even better monitoring and estimation of lifetime of the tower and foundation [184–188].

In latest trend is the smart wireless networks, which have different modules for identification, authentication, and evaluation. This provides information to detect the extent and location of the damage very precisely. The foundation and tower mostly act in the same way, and therefore, it has been observed that the newer technology develops a monitoring system to be able to synchronously detect the conditions of both the components. [189–192]. These discussed systems aim to determine the integrity of the tower and foundation of the wind turbine, as shown in Figure 15.

4.4. Issues of Concern and their Mitigation in Wind Turbines

Since the wind turbine blades are directly exposed to the harsh environment, they are vulnerable to failures. In these environments, wind loads vary constantly, and undergo cyclic fatigue loads under their own weight. Erosion and corrosion experienced by the wind turbines are the results of extreme temperature and humidity changes. Blade failures could also lead to a major economic loss. For example, €1.25 million was exhausted due to the significant downtime and repair costs attributed to the failure of blades in an onshore wind turbine at Dunbar, Scotland in 2005 [193]. The major modes of failure of wind turbine blades include failure of adhesive joints and load-carrying laminates being delaminated. Several non-destructive testing techniques are used to detect these failures. When triggered by the external forces, the vibrational analysis evaluates the dynamic response of blades and hence investigates their health condition [186]. If multiple vibration transducers are used in sequence, that can also be used to detect the damage locations, which is attributed to the reason that fiberglass composite material is used to manufacture the blades of the wind turbine [194]. For the purpose of commercial testing of WT blades, strain gauges are popularly used, which are made up of piezoelectric ceramic materials [195]. These gauges are attached to the surface of the blades for measuring the localized strain arising due to bending and stretching loads [194]. Another technique to monitor structural health monitoring is acoustic emission. When a crack is originated and propagates in the blade, acoustic emission perceives the energy of the elastic waves, which helps in its identification [196]. Other SHM techniques include TFRF, which is developed recently and is trustworthy in both faults as well as damage detection. Along the span direction of the blade, TFRF-based blade SHM measures the dynamic response of the blades. To fulfill this measurement, a distributed strain sensor and high-resolution stereo imaging camera are the two prospective tools, but they require more research for being applicable in the future [194] (Figure 16).

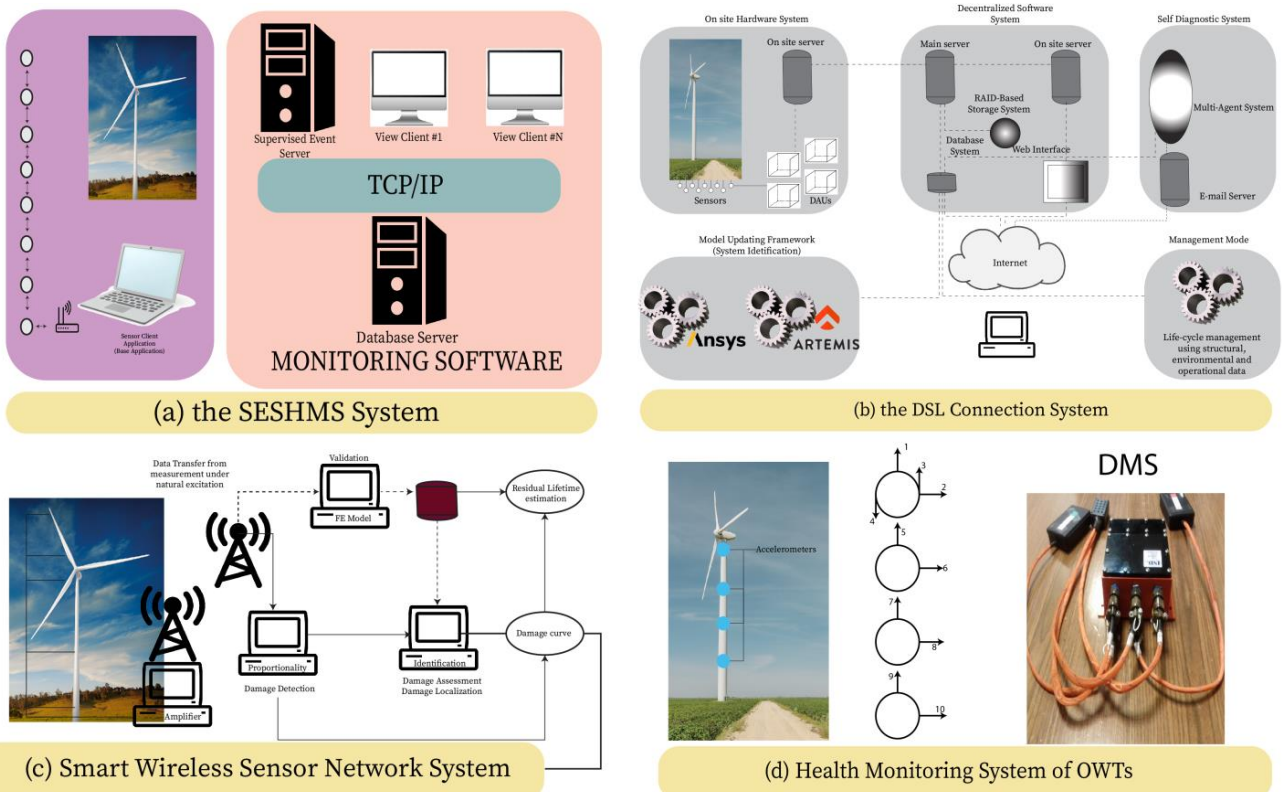


Figure 16. Health monitoring systems of wind turbines [185,189,190,192]. SESHMS: server health monitoring system; WSN: wireless sensor network; DSL: digital subscriber line; DAS: data acquisition system.

5. UAV Systems for Health Monitoring

The Functioning of UAV sensors and receivers and LIDAR data collected from RGIPT Amethi of pipe leakages are shown in Figure 17.

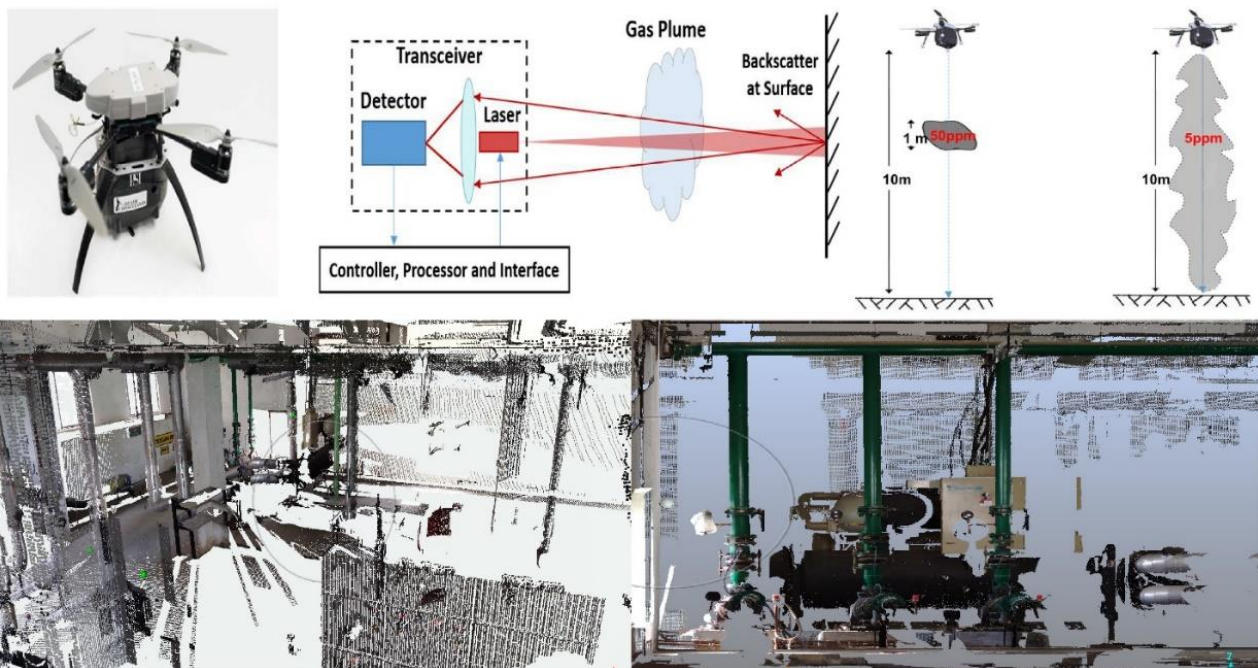


Figure 17. Functioning of UAV sensors and receivers and LIDAR data collected from RGIPT Amethi of pipe leakages. The image is in the form of LIDAR data points.

Leakages in pipelines lead to massive losses; even a leak as small as 1% in a 20-inch-thick pipeline can lead to a loss of more than 500,000 barrels of oil every year. For a solution to this, it is important that these leaks are detected at the right time. One of the few techniques is to use UAV for inspecting a pipeline; this is not only a detection method but is also a method to monitor the environmental conditions in the vicinity of the pipeline. The benefit with using UAVs is that they are capable of covering larger areas in a smaller amount of time as compared to manual inspection. This makes it a cost-effective and time-efficient detection method. The use of UAVs is not only limited to pipelines, and they are now being used in nuclear power plants, chemical plants, etc. Several toxic gases are processed each day in chemical plants across the world, and it is important that not even a pinch of such gases leak out into the atmosphere. Thus, UAVs come in handy, as they efficiently sense even the smallest amount of leakage through the sensors mounted on top of it, which sends signals to the controllers who react accordingly. A payload can be installed on various platforms, which is used to detect gas leakage, and the installation of payload can be seen as a possible solution to detect and then mitigate gas leakage. However, the solution provided by the payload installation is not just concealed to UAVs. In a research study, a UAV was operated at a height of about 40 m from the ground at a speed of 30 km/h for a time period of about 2 h, and the maximum weight of the payload was kept at 5 kg.

At first glance, it was found that only methane gas in the temperature range of 15 to 20 degrees Celsius was leaked out in a pipeline of pressure 1500 psi. To track muffled frequencies and waves, leaks, and different frequencies in metallic machine frameworks, industrial air, vacuum systems, and pressurized gas pipelines, a digital ultrasonic test platform known as SONOCHEK was designed. In particular, the leakage of pressurized air and gas equipment can be very expensive, because more electricity is to be extracted to account for the failure. The frequency of detection is inaudible to human beings and varies from 20 to 100 kHz. Nevertheless, they are easily sensed by SONOCHEK, which is integrated into a complete study, making them audible and noticeable when determining the leakage and assessing the overall amount of damage. To track the leakage problem and other abnormalities, SONOCHEK was designed with two applications: Sonoleak and Sonolevel. In a various range of product configurations, highly engineered airborne and framework-borne detectors and apparels are accessible. Airborne DBS10 sound detector with three separate horns detects and assesses the leakage, insulation damage, partial discharge in pipes and walls, etc. The framework-borne and temperature detector DBS20 with a magnet adapter and 150 mm waveguide (optional) helps in monitoring the ultrasound waves generated by spinning machine parts e.g., gears, tracking of flow conditions. Parabolic detectors help in tracking leakage up to 25 m. A DBT10 ultrasonic emitter can be used to conduct air infiltration tests on windows, doors, and containers. Sometimes, it is used in the building projects of ships and airplanes, rail, and road means of transport. The signal amplitude can be changed based on the sound quality of the environment.

6. Concluding Remarks

The energy industry uses various infrastructures such as reactor, tank, pump, pipeline, plates, turbine, etc. Many of these parts are metallic and undergo wear and tear with time, as they carry fluids of different chemical composition as well as pass through various environmental conditions. The monitoring, repair, and maintenance of this infrastructure is extremely challenging and complex. Corrosion coupons, electrical resistance probes, etc. offer technologies to observe the damages and leaks through gadgets placed inside the conduits. They pass on certain signals and analyze the data to indicate any damage in the infrastructure or help to indicate the rate of corrosion. Generally, the techniques are average in nature and fail to precisely indicate the position of leak or damage. If it works in post processing mode, it fails to indicate the time and extent of leak. The limitation in resolutions for these techniques also restrict them to be used as predictors of damages for various parts of infrastructure. Acoustic emission or ultrasonic-type sensors offers better

precision in terms of location and time of leaks; however, the technology is better applicable to see within. Point OFS, distributed OFS, etc. techniques are novel and can precisely locate the positions of leaks or damages from external positions. They also allow the prediction of damages in time ahead. However, many of these techniques fail to indicate the changes happening within. SCADA and CMS have come up with improved techniques to monitor the external damages at very high frequency. These data are required to be processed and communicated to quickly determine damages to external surfaces. These techniques are used to monitor the structural health of wind farms. UAV-based techniques have come up recently, as they offer the opportunity to scan the infrastructure externally from very close proximity. Various sensors (acoustic emission, thermal, laser, etc.) can be mounted on this airborne platform and used to determine the location of leaks or damages (Table 2).

Over-ground pipelines, reactors, and tanks are easy to monitor; however, complexities increase for underground infrastructures. The extreme conditions that can be found in the oil and gas wellbore pose a certain difficulty in the monitoring of the downhole. This occurs by the presence of carbon dioxide, hydrogen, and mechanical stresses. The OFS can be relied upon for downhole sensing, but with temperatures as high as 300 degrees and hydrogen ingress, the silica fibers are dangerously affected. In addition, instrumental in this can be the presence of water, resulting in long-term instability [101]. The silica hydrogen bond with the adsorption of hydroxyl can result in extrinsic attenuation. As a counter-action to this, a hermetic carbon layer can be added for protection of the silica, but this idea would also fail at the unusually high temperatures encountered, resulting in increased importance of protective coatings [152,153]. The alternatives for silica include sapphire cladding, which is highly expensive. If the cost can be overlooked, it normally eliminates problem and can still work at 1800 degrees. Another challenge is the transfer across long distances and across the hundreds of thousands of miles of pipeline infrastructure with high resolution. There is a common compromise between high-distance transmission and the resolution received. OFS aims to decrease this problem and lead to an optimized [104,154–162].

Acoustic, OFS, and UAV-based techniques offer certain opportunities along with some challenges. It is not possible to monitor the deformations from inside as well as outside using one technology. It is required to place a sensor inside to get an early indication for impending damages or leaks expected in the future. It is required to communicate all the information of deviation or deformation in real time so that the data can be processed and additional or detailed monitoring of leaks (and damage controlling measures) can be instigated instantaneously. A hybrid UAV–OFS–acoustic emission-based monitoring technique can be designed to meet these demands and set up a comprehensive solution for SHM in the energy sector.

Funding: This research received no external funding.

Institutional Review Board Statement: Not applicable.

Informed Consent Statement: Not applicable.

Data Availability Statement: Not applicable.

Conflicts of Interest: The authors declare no conflict of interest.

References

1. Beavers, J.A.; Thompson, N.G.; Technologies, C.C. External corrosion of oil and natural gas pipelines. *ASM Int.* **2006**, *13*, 1–12.
2. Popoola, L.T.; Grema, A.S.; Latinwo, G.K.; Gutti, B. Corrosion problems during oil and gas production and its mitigation. *IJIC* **2013**, *4*, 35. [[CrossRef](#)]
3. Brondel, D.; Edwards, R.; Hayman, A.; Hill, D. Corrosion in the oil industry. *Oilf. Rev.* **2020**, *6*, 4–18.
4. European Commission. The European Semester. Available online: https://ec.europa.eu/info/business-economy-euro/economic-and-fiscal-policy-coordination/eu-economic-governance-monitoring-prevention-correction/european-semester_en (accessed on 18 August 2021).
5. Weiss, P.S. Aiming high. *ACS Nano* **2007**, *1*, 377. [[CrossRef](#)] [[PubMed](#)]
6. Wong, G.; He, S.; Siragam, V.; Bi, Y.; Mbikay, M.; Chretien, M.; Qiu, X. Antiviral activity of quercetin-3- β -O-D-glucoside against Zika virus infection. *Viro. Sin.* **2017**, *32*, 545–547. [[CrossRef](#)] [[PubMed](#)]

7. Gwec. *Global Wind Report*; Global Wind Energy Council: Brussels, Belgium, 2021.
8. Ciang, C.C.; Lee, J.; Bang, H. Structural health monitoring for a wind turbine system: A review of damage detection methods. *Meas. Sci. Technol.* **2008**, *19*, 122001. [[CrossRef](#)]
9. Bagheri, A.; Kourehli, S.S. Damage detection of structures under earthquake excitation using discrete wavelet analysis damage detection of structures under earthquake. *Asian J. Civ. Eng.* **2013**, *14*, 289–304.
10. Pozo, F.; Tibaduiza, D.A.; Vidal, Y. Sensors for structural health monitoring and condition monitoring. *Sensors* **2021**, *21*, 1558. [[CrossRef](#)]
11. Qing, W. Processing high TAN crude: Part I. *Pet. Technol. Q.* **2010**, *4*, 35.
12. Ropital, F. Current and future corrosion challenges for a reliable and sustainable development of the chemical, refinery, and petrochemical industries. *Mater. Corros.* **2009**, *60*, 495–500. [[CrossRef](#)]
13. Turnbull, A. Review of naphthenic acid corrosion in oil refining. *Br. Corros. J.* **1999**, *34*, 125–131.
14. *API RP 571 Damage Mechanisms Affecting Fixed Equipment in the Refining Industry*; American Petroleum Institute: Washington, DC, USA, 2003; pp. 1–12.
15. Wu, X.Q.; Jing, H.M.; Zheng, Y.G.; Yao, Z.M.; Ke, W. Study on high-temperature naphthenic acid corrosion and erosion-corrosion of aluminized carbon steel. *J. Mater. Sci.* **2004**, *9*, 975–985. [[CrossRef](#)]
16. Birring, A.S.; Beissner, R. *Nondestructive Evaluation Methods for It*; Nondestructive Testing Information Analysis Center: San Antonio, TX, USA, 1986.
17. Lozev, M.G.; Smith, R.W.; Grimmett, B.B. Evaluation of methods for detecting and monitoring of corrosion damage in risers. *J. Press. Vessel Technol.* **2005**, *127*, 244–254. [[CrossRef](#)]
18. Liu, Z.; Kleiner, Y. State of the art review of inspection technologies for condition assessment of water pipes. *Measurement* **2013**, *46*, 1–15. [[CrossRef](#)]
19. Bray, D.E. *Nondestructive Evaluation: A Tool in Design, Manufacturing, and Service*; CRC Press: Boca Raton, FL, USA, 2018; ISBN 9781315272993.
20. Shokravi, H.; Shokravi, H.; Bakhary, N.; Heidarrezaei, M.; Rahimian Koloor, S.S.; Petrú, M. Vehicle-assisted techniques for health monitoring of bridges. *Sensors* **2020**, *20*, 3460. [[CrossRef](#)] [[PubMed](#)]
21. Materials, T.; Company, I. *The Materials Information Company*; ASM International: Almere, The Netherlands, 1997; ISBN 0-87170-386-6.
22. Shadravan, A.; Amani, M. Impacts of hydrogen embrittlement on oil and gas wells: Theories behind premature failures. In Proceedings of the SPE Gas & Oil Technology Showcase and Conference, Dubai, United Arab Emirates, 21–23 October 2019.
23. Nagumo, M. Function of hydrogen in embrittlement of high-strength steels. *ISIJ Int.* **2001**, *41*, 590–598. [[CrossRef](#)]
24. Common Causes and Cures of Hydrogen Cracking. Available online: <https://www.fabricatingandmetalworking.com/2014/12/common-causes-cures-hydrogen-cracking> (accessed on 13 February 2021).
25. How to Fix 8 Common Welding Problems with these Easy Steps. Available online: <https://www.welding.com.au/news/view/how-to-fix-8-common-welding-problems-with-these-easy-steps> (accessed on 13 February 2021).
26. Hansen, P.; Alismail, H.; Rander, P.; Browning, B. Pipe mapping with monocular fisheye imagery. In Proceedings of the 2013 IEEE/RSJ International Conference on Intelligent Robots and Systems, Tokyo, Japan, 3–7 November 2013; IEEE: Piscataway, NJ, USA, 2013; pp. 5180–5185.
27. Duran, O.; Althoefer, K.; Seneviratne, L.D. Automated pipe defect detection and categorization using camera/laser-based profiler and artificial neural network. *IEEE Trans. Autom. Sci. Eng.* **2007**, *4*, 118–126. [[CrossRef](#)]
28. Majumder, M.; Gangopadhyay, T.K.; Chakraborty, A.K.; Dasgupta, K.; Bhattacharya, D.K. Fibre Bragg gratings in structural health monitoring—Present status and applications. *Sens. Actuators A Phys.* **2008**, *147*, 150–164. [[CrossRef](#)]
29. Tennyson, R.C.; Banthia, N.; Rivera, E.; Huffman, S.; Sturrock, I. Monitoring structures using long gauge length fibre optic sensors. *Can. J. Civ. Eng.* **2007**, *34*, 422–429. [[CrossRef](#)]
30. Balageas, D.; Fritzen, C.-P.; Güemes, A. *Structural Health Monitoring*; Wiley-ISTE: Hoboken, NJ, USA, 2006.
31. Tonelli, D.; Luchetta, M.; Rossi, F.; Migliorino, P.; Zonta, D. Structural health monitoring based on acoustic emissions: Validation on a prestressed concrete bridge tested to failure. *Sensors* **2020**, *20*, 7272. [[CrossRef](#)]
32. Shokravi, H.; Shokravi, H.; Bakhary, N.; Koloor, S.S.R.; Petrú, M. A Comparative study of the data-driven stochastic subspace methods for health monitoring of structures: A bridge case study. *Appl. Sci.* **2020**, *10*, 3132. [[CrossRef](#)]
33. Barshan, B. Fast processing techniques for accurate ultrasonic range measurements. *Meas. Sci. Technol.* **2000**, *45*, 45–50. [[CrossRef](#)]
34. Jarvis, A.J.C.; Cegla, F.B. Application of the distributed point source method to rough surface scattering and ultrasonic wall thickness measurement. *J. Acoust. Soc. Am.* **2012**, *132*, 1325–1335. [[CrossRef](#)] [[PubMed](#)]
35. Cegla, F.B.; Cawley, P.; Allin, J.; Davies, J. High-temperature (>500 °C) wall thickness monitoring using dry-coupled ultrasonic waveguide transducers. *IEEE Trans. Ultrason. Ferroelectr. Freq. Control* **2011**, *58*, 156–167. [[CrossRef](#)]
36. Kobayashi, M.; Jen, C.K.; Bussiere, J.F.; Wu, K.T. High-temperature integrated and flexible ultrasonic transducers for nondestructive testing. *NDT E Int.* **2009**, *42*, 157–161. [[CrossRef](#)]
37. Bartoli, I. *Structural Health Monitoring by Ultrasonic Guided Waves*; UC San Diego: San Diego, CA, USA, 2007.
38. Rose, J.L. Ultrasonic guided waves in structural health monitoring. *Key Eng. Mater.* **2004**, *270*, 14–21. [[CrossRef](#)]
39. Rose, J.L.; Soley, L.E. Ultrasonic guided waves for anomaly detection in aircraft components. *Mater. Eval.* **2000**, *58*, 1080–1086.

40. Hongerholt, D.D. Summary of results from an ultrasonic in-flight wing ice detection system. *AIP Conf. Proc.* **2003**, *615*, 1023–1028. [[CrossRef](#)]
41. Rose, J.; Zhu, W.; Zaidi, M. Ultrasonic NDT of titanium diffusion bonding with guided waves. *Undefined* **1998**, *56*, 535–539.
42. Hay, T.; Rose, J.L. Skin to Honeycomb Core delamination Detection with Guided Waves. In Proceedings of the 15th World Conference on Non-Destructive Testing (WCNDT), Rome, Italy, 15–21 October 2000; pp. 1–14.
43. ETHICON™ Energy | Energy Sealing & Dissecting | J&J Medical Devices. Available online: <https://www.jnjmedicaldevices.com/en-US/product-family/energy-sealing-dissecting> (accessed on 18 August 2021).
44. Cawley, P.; Lowe, M.J.S.; Alleyne, D.N.; Pavlakovic, B.; Wilcox, P. Practical long range guided wave testing: Applications to pipes and rail. *Mater. Eval.* **2003**, *61*, 66–74.
45. Elastic Wave Analysis for Broken Rail Detection. Available online: <https://www.ndt.net/article/wcndt00/papers/idn270/idn270.htm> (accessed on 19 August 2021).
46. Hayashi, T.; Song, W.J.; Rose, J.L. Guided wave dispersion curves for a bar with an arbitrary cross-section, a rod and rail example. *Ultrasonics* **2003**, *41*, 175–183. [[CrossRef](#)]
47. Rose, J.L. Ultrasonic inspection of adhesive bonds. In *Adhesion Science and Engineering*; Pocius, A.V., Dillard, D.A., Eds.; Elsevier: Amsterdam, The Netherlands, 2002; pp. 699–724. [[CrossRef](#)]
48. Sun, Z.; Rose, L.J.; Zaidi, M. A phased array guided wave approach to adhesive bonding structural integrity analysis—Penn State. *Mater. Eval.* **2003**, *61*, 941–946.
49. Song, W.J.; Rose, J.L.; Galán, J.M.; Abascal, R. Ultrasonic guided wave scattering in a plate overlap. *IEEE Trans. Ultrason. Ferroelectr. Freq. Control* **2005**, *52*, 892–903. [[CrossRef](#)]
50. Rose, J.L.; Avioli, M.J.; Mudge, P.; Sanderson, R. Guided wave inspection potential of defects in rail. *NDT E Int.* **2004**, *37*, 153–161. [[CrossRef](#)]
51. Koch, G.H.; Brongers, M.P.H.; Thompson, N.G.; Virmani, Y.P.; Payer, J.H. *Corrosion Costs and Preventive Strategies in the United States*; NACE International: Houston, TX, USA, 1998; pp. 1–10.
52. Wright, R.F.; English, R.; Egbu, J.C.; Baltrus, J.; Ziomek-Moroz, M.; Ohodnicki, P.R. Fe thin film-coated optics for corrosion monitoring: Optical and electrochemical studies. *JOM* **2021**, *73*, 655–664. [[CrossRef](#)]
53. Wright, R.F.; Brand, E.R.; Ziomek-Moroz, M.; Tylczak, J.H.; Ohodnicki, P.R. Effect of HCO_3^- on electrochemical kinetics of carbon steel corrosion in CO_2 -saturated brines. *Electrochim. Acta* **2018**, *290*, 626–638. [[CrossRef](#)]
54. Nestic, S.; Postlethwaite, J.; Olsen, S. An electrochemical model for prediction of corrosion of mild steel in aqueous carbon dioxide solutions. *Corrosion* **1996**, *52*, 280–294. [[CrossRef](#)]
55. Sun, W.; Nestic, S. A mechanistic model of H_2S corrosion of mild steel. In Proceedings of the Corrosion 2007, Nashville, TN, USA, 11–15 March 2007; p. 07655. [[CrossRef](#)]
56. Zheng, Y.; Ning, J.; Brown, B.; Nešić, S. Electrochemical model of mild steel corrosion in a mixed $\text{H}_2\text{S}/\text{CO}_2$ aqueous environment in the absence of protective corrosion product layers. *Corrosion* **2015**, *71*, 316–325. [[CrossRef](#)]
57. Feng, R.; Beck, J.R.; Hall, D.M.; Buyuksagis, A.; Ziomek-Moroz, M.; Lvov, S.N. Effects of CO_2 and H_2S on corrosion of martensitic steels in brines at low temperature. *Corrosion* **2018**, *74*, 276–287. [[CrossRef](#)]
58. Feng, R.; Beck, J.; Ziomek-Moroz, M.; Lvov, S.N. Electrochemical corrosion of ultra-high strength carbon steel in alkaline brines containing hydrogen sulfide. *Electrochim. Acta* **2016**, *212*, 998–1009. [[CrossRef](#)]
59. Feng, R.; Beck, J.; Ziomek-Moroz, M.; Lvov, S.N. High-temperature electrochemical corrosion of ultra-high strength carbon steel in H_2S -Containing Alkaline Brines. *Electrochim. Acta* **2017**, *241*, 341–352. [[CrossRef](#)]
60. Heidersbach, R. *Metallurgy and Corrosion Control in Oil and Gas Production*; Wiley: Hoboken, NJ, USA, 2018; ISBN 9781119252054.
61. Ziomek-Moroz, M. Environmentally assisted cracking of drill pipes in deep drilling oil and natural gas wells. *J. Mater. Eng. Perform.* **2012**, *21*, 1061–1069. [[CrossRef](#)]
62. Iverson, W.P. Microbial corrosion of metals. *Adv. Appl. Microbiol.* **1987**, *32*, 1–36. [[CrossRef](#)]
63. Craig, B. Deep oil and gas well construction. *Adv. Mater. Process.* **2008**, *166*, 33.
64. NACE Intl Task Goup. Technique for monitoring corrosion and related parameters in field applications. *NACE Int. Publ.* **2012**, *199*, 1–41.
65. Agarwala, V.S.; Reed, P.L.; Ahmad, S. Corrosion detection and monitoring—A review. In Proceedings of the Corrosion 2000, Orlando, FL, USA, 26–31 March 2000.
66. Tullmin, M.A.A.; Roberge, P.R.; Little, M.A. Sensors for Aircraft Corrosion—Review and Future Developments. In Proceedings of the Corrosion 1997, New Orleans, LA, USA, 9–14 March 1997.
67. Qi, X.; Gelling, J.V. A Review of different sensors applied to corrosion detection and monitoring. *Recent Patents Corros. Sci.* **2011**, *1*, 1–7. [[CrossRef](#)]
68. ASTM G4-01 Standard Guide for Conducting Corrosion Tests in Field Applications. Available online: <https://www.astm.org/DATABASE.CART/HISTORICAL/G4-01.htm> (accessed on 18 August 2021).
69. Kuang, F.; Jinna, J.; Zou, C.; Shi, T.; Wang, Y.; Zhang, S.; Xu, H.; Zhang, J. Electrochemical methods for corrosion monitoring: A survey of recent patents. *Recent Patents Corros. Sci.* **2010**, *2*, 34–39. [[CrossRef](#)]
70. Pallarés, F.J.; Betti, M.; Bartoli, G.; Pallarés, L. Structural health monitoring (SHM) and Nondestructive testing (NDT) of slender masonry structures: A practical review. *Constr. Build. Mater.* **2021**, *297*, 123768. [[CrossRef](#)]

71. Wright, R.F.; Lu, P.; Devkota, J.; Lu, F.; Ziomek-Moroz, M.; Ohodnicki, P.R. Review on corrosion sensors for structural health monitoring of oil and natural gas infrastructure. In *Proceedings of the Smart Structures and NDE for Energy Systems and Industry 4.0*; Niezrecki, C., Meyendorf, N.G., Gath, K., Eds.; SPIE: Bellingham, WA, USA, 2019; Volume 10973, p. 22.
72. LPR Probe 7012/7022—Cosasco. Available online: <https://www.cosasco.com/product/lpr-probe-7012-7022> (accessed on 18 August 2021).
73. Sridhar, N.; Yang, L. Coupled multielectrode array systems and sensors for real-time corrosion monitoring—A review. In *Proceedings of the Corrosion 2006*, San Diego, CA, USA, 12–16 March 2006.
74. Chiang, K.T.; Yang, L. High-temperature electrochemical sensor for online corrosion monitoring. In *Proceedings of the Corrosion 2010*, San Antonio, TX, USA, 14–18 March 2010; pp. 095002–095008. [[CrossRef](#)]
75. Yang, L. Coupled multielectrode array sensors for localized corrosion monitoring. In *Proceedings of the NACE TEG 97 Technical Information Exchange*, Houston, TX, USA, 13 March 2011.
76. Beck, J.; Hall, D.M.; Ziomek-Moroz, M.; Lvov, S.N. Membrane-based electrochemical sensor for corrosion monitoring in natural gas pipelines. *ECS Trans.* **2017**, *77*, 681–691. [[CrossRef](#)]
77. Hall, D.M.; Duffy, T.; Ziomek-Moroz, M.; Lvov, S.N. Electrochemical impedance spectroscopy and finite element analysis modeling of a 4-electrode humidity sensor for natural gas transportation pipelines. *Rev. Sci. Instrum.* **2019**, *90*, 015005. [[CrossRef](#)] [[PubMed](#)]
78. Rodríguez-Olivares, N.A.; Cruz-Cruz, J.V.; Gómez-Hernández, A.; Hernández-Alvarado, R.; Nava-Balanzar, L.; Salgado-Jiménez, T.; Soto-Cajiga, J.A. Improvement of ultrasonic pulse generator for automatic pipeline inspection. *Sensors* **2018**, *18*, 2950. [[CrossRef](#)]
79. Cegla, F. Ultrasonic Monitoring of Corrosion with Permanently Installed Sensors (PIMS). In *Sensors, Algorithms and Applications for Structural Health Monitoring*; Chapuis, B., Sjerve, E., Eds.; Springer: Berlin/Heidelberg, Germany, 2018; pp. 13–20. [[CrossRef](#)]
80. Lakestani, F.; Coste, J.F.; Denis, R. Application of ultrasonic Rayleigh waves to thickness measurement of metallic coatings. *NDT E Int.* **1995**, *28*, 171–178. [[CrossRef](#)]
81. Ali, S.H.; Zaid, M.; Abdullah, M.; Khan, T.M.R. SHM of Concrete Bridge Structures using Wireless Sensor Networks. In *Proceedings of the Smart SysTech 2018: European Conference on Smart Objects, Systems and Technologies*, Dresden, Germany, 12–13 June 2018; pp. 1–6.
82. Rao, B.P.C. Magnetic flux leakage technique: Basics. *J. Nondestruct. Test. Eval.* **2012**, *11*, 7–17.
83. Shi, Y.; Zhang, C.; Li, R.; Cai, M.; Jia, G. Theory and application of magnetic flux leakage pipeline detection. *Sensors* **2015**, *15*, 31036–31055. [[CrossRef](#)]
84. Qiao, G.; Zhou, Z.; Ou, J. Thin Fe-C alloy solid film based fiber optic corrosion sensor. In *Proceedings of the 1st IEEE International Conference on Nano/Micro Engineered and Molecular Systems (NEMS '06)*, Zhuhai, China, 18–21 January 2006; pp. 541–544. [[CrossRef](#)]
85. Leung, C.K.Y.; Wan, K.T.; Chen, L. A novel optical fiber sensor for steel corrosion in concrete structures. *Sensors* **2008**, *8*, 1960–1976. [[CrossRef](#)] [[PubMed](#)]
86. Dong, S.; Liao, Y.; Tian, Q.; Luo, Y.; Qiu, Z.; Song, S. Optical and electrochemical measurements for optical fibre corrosion sensing techniques. *Corros. Sci.* **2006**, *48*, 1746–1756. [[CrossRef](#)]
87. Vengsarkar, A.M.; Bhatia, V. Optical fiber long-period grating sensors. *Opt. Lett.* **1996**, *21*, 692–694. [[CrossRef](#)]
88. James, S.W.; Tatam, R.P. Optical fibre long-period grating sensors: Characteristics and application. *Meas. Sci. Technol.* **2003**, *14*, 49–61. [[CrossRef](#)]
89. Tang, F.; Chen, G.; Tang, Y.; Bao, Y.; Chen, Y. A Fe-C coated long-period fiber grating sensor for corrosion-induced mass loss measurement. *Opt. Lett.* **2016**, *41*, 2306–2309. [[CrossRef](#)]
90. Guo, C.; Fan, L.; Wu, C.; Chen, G.; Li, W. Ultrasensitive LPFG corrosion sensor with Fe-C coating electroplated on a Gr/AgNW film. *Sens. Actuators B Chem.* **2019**, *283*, 334–342. [[CrossRef](#)]
91. Hou, Q.; Ren, L.; Jiao, W.; Zou, P.; Song, G. An improved negative pressure wave method for natural gas pipeline leak location using FBG based strain sensor and wavelet transform. *Math. Probl. Eng.* **2013**, *2013*, 278794. [[CrossRef](#)]
92. Wang, J.; Grattan, K.T.V.; Zhao, L.; Sun, T.; Liu, T.; Li, Z. Novel negative pressure wave-based pipeline leak detection system using fiber bragg grating-based pressure sensors. *J. Light. Technol.* **2017**, *35*, 3366–3373. [[CrossRef](#)]
93. Freire, J.L.F.; Perrut, V.A.; Braga, A.M.B.; Vieira, R.D.; Ribeiro, A.S.; Rosas, M.A.P. Use of FBG strain gages on a pipeline specimen repaired with a CFRE composite. *Exp. Tech.* **2015**, *395*, 70–79. [[CrossRef](#)]
94. Xu, J.; Yang, D.; Qin, C.; Jiang, Y.; Sheng, L.; Jia, X.; Bai, Y.; Shen, X.; Wang, H.; Deng, X.; et al. Study and test of a new bundle-structure riser stress monitoring sensor based on FBG. *Sensors* **2015**, *15*, 29648–29660. [[CrossRef](#)]
95. Morrison, D.G.; Dean, J.R. Apparatuses and Methods for Monitoring Stress in Steel Catenary Risers. U.S. Patent US7194913B2, 27 March 2007.
96. Brower, D.; Prescott, N. Real time subsea monitoring and control smart field solutions. In *Proceedings of the Subsea Rio 2004 Conference*, Rio de Janeiro, Brazil, 3 June 2004.
97. Yulianti, I.; Supa'at, A.S.M.; Idrus, S.M.; Kurdi, O.; Anwar, M.R.S. Sensitivity improvement of a fiber Bragg grating pH sensor with elastomeric coating. *Meas. Sci. Technol.* **2011**, *23*, 15104. [[CrossRef](#)]
98. Tahhan, S.R.; Chen, R.Z.; Huang, S.; Hajim, K.I.; Chen, K.P. Fabrication of fiber bragg grating coating with TiO₂ nanostructured metal oxide for refractive index sensor. *J. Nanotechnol.* **2017**, *2017*, 2791282. [[CrossRef](#)]

99. Yeo, T.L.; Sun, T.; Grattan, K.T.V.; Parry, D.; Lade, R.; Powell, B.D. Characterisation of a polymer-coated fibre Bragg grating sensor for relative humidity sensing. *Sens. Actuators B Chem.* **2005**, *1*, 148–156. [[CrossRef](#)]
100. Ukil, A.; Braendle, H.; Krippner, P. Distributed temperature sensing: Review of technology and applications. *IEEE Sens. J.* **2012**, *12*, 885–892. [[CrossRef](#)]
101. Yamate, T.; Fujisawa, G.; Ikegami, T. Optical sensors for the exploration of oil and gas. *J. Light. Technol.* **2017**, *35*, 3538–3545. [[CrossRef](#)]
102. Mirzaei, A.; Bahrampour, A.R.; Taraz, M.; Bahrampour, A.; Bahrampour, M.J.; Ahmadi Foroushani, S.M. Transient response of buried oil pipelines fiber optic leak detector based on the distributed temperature measurement. *Int. J. Heat Mass Transf.* **2013**, *65*, 110–122. [[CrossRef](#)]
103. Stajanca, P.; Chruscicki, S.; Homann, T.; Seifert, S.; Schmidt, D.; Habib, A. Detection of leak-induced pipeline vibrations using fiber—Optic distributed acoustic sensing. *Sensors* **2018**, *18*, 2841. [[CrossRef](#)] [[PubMed](#)]
104. Muanenda, Y. Recent advances in distributed acoustic sensing based on phase-sensitive optical time domain reflectometry. *J. Sens.* **2018**, *2018*, 3897873. [[CrossRef](#)]
105. Joe, H.E.; Yun, H.; Jo, S.H.; Jun, M.B.G.; Min, B.K. A review on optical fiber sensors for environmental monitoring. *Int. J. Precis. Eng. Manuf. Green Technol.* **2018**, *5*, 173–191. [[CrossRef](#)]
106. Zhang, Y.; Peng, H.; Qian, X.; Zhang, Y.; An, G.; Zhao, Y. Recent advancements in optical fiber hydrogen sensors. *Sens. Actuators B Chem.* **2017**, *244*, 393–416. [[CrossRef](#)]
107. Lu, P.; Ziomek-moroz, M.; Buric, M.P. A Multifunctional Fiber Optic Sensor for Internal Corrosion Monitoring in Natural Gas Transmission Pipelines. In Proceedings of the NACE-International Corrosion Conference Series, Phoenix, AZ, USA, 15–19 April 2018.
108. Knight, J.C.; Broeng, J.; Birks, T.A.; Russell, P.S.J. Photonic band gap guidance in optical fibers. *Science* **1998**, *282*, 1476–1478. [[CrossRef](#)] [[PubMed](#)]
109. Monro, T.M.; Belardi, W.; Furusawa, K.; Baggett, J.C.; Broderick, N.G.R.; Richardson, D.J. Sensing with microstructured optical fibres. *Meas. Sci. Technol.* **2001**, *12*, 854–858. [[CrossRef](#)]
110. Pinto, A.M.R.; Lopez-Amo, M. Photonic crystal fibers for sensing applications. *J. Sens.* **2012**, *2012*, 1–21. [[CrossRef](#)]
111. Atkin, D.M.; Knight, J.C.; Russell, P.S.J.; Birks, T.A. All-silica single-mode optical fiber with photonic crystal cladding. *Opt. Lett.* **1996**, *21*, 1547–1549. [[CrossRef](#)]
112. Hingerl, F.F.; Marpu, S.; Guzman, N.; Benson, S.M.; Delgado-Alonso, J. Development and testing of a new fiber optic system for monitoring CO₂ solubility in aqueous high-pressure geological systems. *Energy Procedia* **2014**, *63*, 4134–4144. [[CrossRef](#)]
113. George, A.K.; Hand, D.P.; Reid, D.T.; Knight, J.C.; Stone, J.M.; Gayraud, N.; MacPherson, W.N.; Kornaszewski, L. Mid-infrared methane detection in a photonic bandgap fiber using a broadband optical parametric oscillator. *Opt. Express* **2007**, *15*, 11219–11224. [[CrossRef](#)]
114. Carvalho, J.P.; Lehmann, H.; Bartelt, H.; Magalhães, F.; Amezcua-Correa, R.; Santos, J.L.; Van Roosbroeck, J.; Araújo, F.M.; Ferreira, L.A.; Knight, J.C. Remote system for detection of low-levels of methane based on photonic crystal fibres and wavelength modulation spectroscopy. *J. Sens.* **2009**, *2009*, 1–10. [[CrossRef](#)]
115. Tang, D.L.; He, S.; Dai, B.; Tang, X.H. Detection H₂S mixed with natural gas using hollow-core photonic bandgap fiber. *Optik* **2014**, *125*, 2547–2549. [[CrossRef](#)]
116. Hoo, Y.L.; Jin, W.; Shi, C.; Ho, H.L.; Wang, D.N.; Ruan, S.C. Design and modeling of a photonic crystal fiber gas sensor. *Appl. Opt.* **2003**, *42*, 3509. [[CrossRef](#)]
117. Quintero, S.M.M.; Valente, L.C.G.; Gomes, M.S.D.P.; da Silva, H.G.; de Souza, B.C.; Morikawa, S.R.K. All-fiber CO₂ sensor using hollow core PCF operating in the 2 μm Region. *Sensors* **2018**, *18*, 4393. [[CrossRef](#)]
118. Ding, L.; Li, Z.; Ding, Q.; Shen, X.; Yuan, Y.; Huang, J. Microstructured optical fiber based chloride ion sensing method for concrete health monitoring. *Sens. Actuators B Chem.* **2018**, *260*, 763–769. [[CrossRef](#)]
119. Wright, R.F.; Egbu, J.; Lu, P.; Buric, M.; Ziomek-Moroz, M.; Ohodnicki, P.R. Electrolessly coated optical fibers for distributed corrosion monitoring. *NACE-Int. Corros. Conf. Ser.* **2019**, *2019*, 13499.
120. Addanki, S.; Amiri, I.S.; Yupapin, P. Review of optical fibers-introduction and applications in fiber lasers. *Results Phys.* **2018**, *10*, 743–750. [[CrossRef](#)]
121. Thomas, P.J.; Hellevang, J.O. A high response polyimide fiber optic sensor for distributed humidity measurements. *Sens. Actuators B Chem.* **2018**, *270*, 417–423. [[CrossRef](#)]
122. Wright, R.; Badar, M.; Egbu, J.C.; Lu, P.; Buric, M.P.; Ohodnicki, P.R. Fully distributed optical fiber sensor for water and humidity monitoring. In Proceedings of the Fiber Optic Sensors and Applications XVI, Baltimore, MD, USA, 16–17 April 2019; Sanders, G.A., Lieberman, R.A., Scheel, I.U., Eds.; SPIE: Bellingham, WA, USA, 2019; Volume 11000, p. 6.
123. Lu, X.; Thomas, P.J.; Hellevang, J.O. A review of methods for fibre-optic distributed chemical sensing. *Sensors* **2019**, *19*, 2876. [[CrossRef](#)]
124. Wang, C.; Ohodnicki, P.R.; Su, X.; Keller, M.; Brown, T.D.; Baltrus, J.P. Novel silica surface charge density mediated control of the optical properties of embedded optically active materials and its application for fiber optic pH sensing at elevated temperatures. *Nanoscale* **2015**, *7*, 2527–2535. [[CrossRef](#)]
125. Mishra, S.K.; Gupta, B.D. Surface plasmon resonance based fiber optic pH sensor utilizing Ag/ITO/Al/hydrogel layers. *Analyst* **2013**, *138*, 2640–2646. [[CrossRef](#)] [[PubMed](#)]

126. Rivero, P.J.; Goicoechea, J.; Hernaez, M.; Socorro, A.B.; Matias, I.R.; Arregui, F.J. Optical fiber resonance-based pH sensors using gold nanoparticles into polymeric layer-by-layer coatings. *Microsyst. Technol.* **2016**, *22*, 1821–1829. [[CrossRef](#)]
127. Miled, O.B.; Grosso, D.; Sanchez, C.; Livage, J. An optical fibre pH sensor based on dye doped mesostructured silica. *J. Phys. Chem. Solids* **2004**, *65*, 1751–1755. [[CrossRef](#)]
128. Gupta, B.D.; Sharma, S. A long-range fiber optic pH sensor prepared by dye doped sol-gel immobilization technique. *Opt. Commun.* **1998**, *154*, 282–284. [[CrossRef](#)]
129. Beltrán-Pérez, G.; López-Huerta, F.; Muñoz-Aguirre, S.; Castillo-Mixcóatl, J.; Palomino-Merino, R.; Lozada-Morales, R.; Portillo-Moreno, O. Fabrication and characterization of an optical fiber pH sensor using sol-gel deposited TiO₂ film doped with organic dyes. *Sens. Actuators B Chem.* **2006**, *120*, 74–78. [[CrossRef](#)]
130. Schyrr, B.; Pasche, S.; Scolan, E.; Ischer, R.; Ferrario, D.; Porchet, J.A.; Voirin, G. Development of a polymer optical fiber pH sensor for on-body monitoring application. *Sens. Actuators B Chem.* **2014**, *194*, 238–248. [[CrossRef](#)]
131. Gupta, B.D.; Sharma, D.K. Evanescent wave absorption based fiber optic pH sensor prepared by dye doped sol-gel immobilization technique. *Opt. Commun.* **1997**, *140*, 32–35. [[CrossRef](#)]
132. Alvarado-Méndez, E.; Rojas-Laguna, R.; Andrade-Lucio, J.A.; Hernández-Cruz, D.; Lessard, R.A.; Aviña-Cervantes, J.G. Design and characterization of pH sensor based on sol-gel silica layer on plastic optical fiber. *Sens. Actuators B Chem.* **2005**, *106*, 518–522. [[CrossRef](#)]
133. Nguyen, T.H.; Venugopala, T.; Chen, S.; Sun, T.; Grattan, K.T.V.; Taylor, S.E.; Basheer, P.A.M.; Long, A.E. Fluorescence based fibre optic pH sensor for the pH 10–13 range suitable for corrosion monitoring in concrete structures. *Sens. Actuators B Chem.* **2014**, *191*, 498–507. [[CrossRef](#)]
134. Ton, X.-A.; Acha, V.; Bonomi, P.; Bui, B.T.S.; Haupt, K. A disposable evanescent wave fiber optic sensor coated with a molecularly imprinted polymer as a selective fluorescence probe. *Biosens. Bioelectron.* **2015**, *64*, 359–366. [[CrossRef](#)]
135. Rosenberg, M.; Laursen, B.W.; Frankær, C.G.; Sørensen, T.J. A fluorescence intensity ratiometric fiber optics-based chemical sensor for monitoring pH. *Adv. Mater. Technol.* **2018**, *3*, 1800205. [[CrossRef](#)]
136. Wallace, P.A.; Campbell, M.; Yang, Y.; Holmes-Smith, A.S.; Uttamlal, M. A distributed optical fibre fluorosensor for pH measurement. *J. Lumin.* **1997**, *72–74*, 1017–1019. [[CrossRef](#)]
137. Nguyen, T.H.; Venugopalan, T.; Sun, T.; Grattan, K.T.V. Intrinsic fiber optic pH sensor for measurement of pH values in the range of 0.5–6. *IEEE Sens. J.* **2016**, *16*, 881–887. [[CrossRef](#)]
138. Shao, L.-Y.; Yin, M.-J.; Tam, H.-Y.; Albert, J. Fiber optic pH sensor with self-assembled polymer multilayer nanocoatings. *Sensors* **2013**, *13*, 1425–1434. [[CrossRef](#)]
139. Jin, Z.; Su, Y.; Duan, Y. An improved optical pH sensor based on polyaniline. *Sens. Actuators B Chem.* **2000**, *71*, 118–122. [[CrossRef](#)]
140. Moutsipoulou, A.; Andreopoulou, A.K.; Lainioti, G.; Bokias, G.; Voyiatzis, G.; Kallitsis, J.K. Quinoline-functionalized cross-linked poly(vinyl acetate) and poly(vinyl alcohol) nanoparticles as potential pH-responsive luminescent sensors. *Sens. Actuators B Chem.* **2015**, *211*, 235–244. [[CrossRef](#)]
141. Rivero, P.J.; Goicoechea, J.; Arregui, F.J. Optical fiber sensors based on polymeric sensitive coatings. *Polymers* **2018**, *10*, 280. [[CrossRef](#)] [[PubMed](#)]
142. Singh, S.; Gupta, B.D. Fabrication and characterization of a highly sensitive surface plasmon resonance based fiber optic pH sensor utilizing high index layer and smart hydrogel. *Sens. Actuators B Chem.* **2012**, *173*, 268–273. [[CrossRef](#)]
143. Pathak, A.K.; Singh, V.K. A wide range and highly sensitive optical fiber pH sensor using polyacrylamide hydrogel. *Opt. Fiber Technol.* **2017**, *39*, 43–48. [[CrossRef](#)]
144. Zhao, Y.; Lei, M.; Liu, S.X.; Zhao, Q. Smart hydrogel-based optical fiber SPR sensor for pH measurements. *Sens. Actuators B Chem.* **2018**, *261*, 226–232. [[CrossRef](#)]
145. Richter, A.; Paschew, G.; Klatt, S.; Lienig, J.; Arndt, K.-F.; Adler, H.-J.P. Review on hydrogel-based pH sensors and microsensors. *Sensors* **2008**, *8*, 561–581. [[CrossRef](#)]
146. Ohodnicki, P.R., Jr.; Wang, C. Optical waveguide modeling of refractive index mediated pH responses in silica nanocomposite thin film based fiber optic sensors. *J. Appl. Phys.* **2016**, *119*, 064502. [[CrossRef](#)]
147. Lin, J. Recent development and applications of optical and fiber-optic pH sensors. *TrAC-Trends Anal. Chem.* **2000**, *19*, 541–552. [[CrossRef](#)]
148. Kocak, G.; Tuncer, C.; Bütün, V. pH-Responsive polymers. *Polym. Chem.* **2016**, *8*, 144–176. [[CrossRef](#)]
149. Qian, Y.; Zhao, Y.; Wu, Q.; Yang, Y. Review of salinity measurement technology based on optical fiber sensor. *Sens. Actuators B Chem.* **2018**, *260*, 86–105. [[CrossRef](#)]
150. Rahman, H.A.; Harun, S.W.; Yasin, M.; Phang, S.W.; Damanhuri, S.S.A.; Arof, H.; Ahmad, H. Tapered plastic multimode fiber sensor for salinity detection. *Sens. Actuators A Phys.* **2011**, *171*, 219–222. [[CrossRef](#)]
151. Wang, J.; Chen, B. Experimental research of optical fiber sensor for salinity measurement. *Sens. Actuators A Phys.* **2012**, *184*, 53–56. [[CrossRef](#)]
152. Lemaire, P.J. Hydrogen-induced losses and their effects on optical fiber reliability. *Fiber Opt. Reliab. Test. A Crit. Rev.* **1993**, *10272*, 1027207. [[CrossRef](#)]
153. 50 Graded-Index OM2-Bend-Insensitive Multimode Optical Fiber. Available online: www.ofsoptics.com (accessed on 18 August 2021).

154. Chen, H.; Buric, M.; Ohodnicki, P.R.; Nakano, J.; Liu, B.; Chorpene, B.T. Review and perspective: Sapphire optical fiber cladding development for harsh environment sensing. *Appl. Phys. Rev.* **2018**, *5*, 011102. [[CrossRef](#)]
155. Dong, Y.; Chen, L.; Bao, X. Extending the sensing range of Brillouin optical time-domain analysis combining frequency-division multiplexing and in-line EDFAs. *J. Light. Technol.* **2012**, *30*, 1161–1167. [[CrossRef](#)]
156. Loayssa, A.; Urricelqui, J.; Mompó, J.J. Brillouin optical time-domain analysis sensor with pump pulse amplification. *Opt. Express* **2016**, *24*, 12672–12681. [[CrossRef](#)]
157. Angulo-Vinuesa, X.; Martin-Lopez, S.; Corredera, P.; Gonzalez-Herraez, M. Raman-assisted Brillouin optical time-domain analysis with sub-meter resolution over 100 km. *Opt. Express* **2012**, *20*, 12147. [[CrossRef](#)]
158. Moore, J.; Froggatt, M. High-spatial-resolution distributed strain measurement in optical fiber with Rayleigh scatter. *Appl. Opt.* **1998**, *37*, 1735–1740. [[CrossRef](#)]
159. Kreger, S.T.; Gifford, D.K.; Froggatt, M.E.; Soller, B.J.; Wolfe, M.S. High resolution distributed strain or temperature measurements in single- and multi-mode fiber using swept-wavelength interferometry. In Proceedings of the Optical Fiber Sensors 2006, Cancun, Mexico, 23–27 October 2006. [[CrossRef](#)]
160. Ding, Z.; Yang, D.; Du, Y.; Liu, K.; Zhou, Y.; Zhang, R.; Xu, Z.; Jiang, J.; Liu, T. Distributed strain and temperature discrimination using two types of fiber in OFDR. *IEEE Photonics J.* **2016**, *8*, 1–8. [[CrossRef](#)]
161. Zhou, D.-P.; Li, W.; Chen, L.; Bao, X. Distributed temperature and strain discrimination with stimulated Brillouin scattering and Rayleigh backscatter in an optical fiber. *Sensors* **2013**, *13*, 1836–1845. [[CrossRef](#)]
162. Peng, F.; Wu, H.; Jia, X.-H.; Rao, Y.-J.; Peng, Z.-P.; Wang, Z.-N. Ultra-long high-sensitivity Φ -OTDR for high spatial resolution intrusion detection of pipelines. *Opt. Express* **2014**, *22*, 13804–13810. [[CrossRef](#)] [[PubMed](#)]
163. Salameh, J.P.; Cauet, S.; Etien, E.; Sakout, A.; Rambault, L. Gearbox condition monitoring in wind turbines: A review. *Mech. Syst. Signal Process.* **2018**, *111*, 251–264. [[CrossRef](#)]
164. Schlechtingen, M.; Santos, I.F.; Achiche, S. Wind turbine condition monitoring based on SCADA data using normal behavior models. Part 1: System description. *Appl. Soft Comput. J.* **2013**, *13*, 259–270. [[CrossRef](#)]
165. Schlechtingen, M.; Santos, I.F. Wind turbine condition monitoring based on SCADA data using normal behavior models. Part 2: Application examples. *Appl. Soft Comput. J.* **2014**, *14*, 447–460. [[CrossRef](#)]
166. Song, Z.; Zhang, Z.; Jiang, Y.; Zhu, J. Wind turbine health state monitoring based on a Bayesian data-driven approach. *Renew. Energy* **2018**, *125*, 172–181. [[CrossRef](#)]
167. Yang, W.; Court, R.; Jiang, J. Wind turbine condition monitoring by the approach of SCADA data analysis. *Renew. Energy* **2013**, *53*, 365–376. [[CrossRef](#)]
168. Nie, M.; Wang, L. Review of condition monitoring and fault diagnosis technologies for wind turbine gearbox. *Procedia CIRP* **2013**, *11*, 287–290. [[CrossRef](#)]
169. Romero, A.; Soua, S.; Gan, T.-H.; Wang, B. Condition monitoring of a wind turbine drive train based on its power dependant vibrations. *Renew. Energy* **2018**, *123*, 817–827. [[CrossRef](#)]
170. Wymore, M.L.; Van Dam, J.E.; Ceylan, H.; Qiao, D. A survey of health monitoring systems for wind turbines. *Renew. Sustain. Energy Rev.* **2015**, *52*, 976–990. [[CrossRef](#)]
171. Lu, B.; Li, Y.; Wu, X.; Yang, Z. A review of recent advances in wind turbine condition monitoring and fault diagnosis. In Proceedings of the 2009 IEEE Power Electronics and Machines in Wind Applications, Lincoln, NE, USA, 24–26 June 2009; IEEE: Piscataway, NJ, USA, 2009; pp. 1–7.
172. Sutherland, H.; Beattie, A.; Hansche, B.; Musial, W.; Allread, J.; Johnson, J.; Summers, M. *The Application of Non-Destructive Techniques to the Testing of a Wind Turbine Blade*; USDOE: Washington, DC, USA, 1994. [[CrossRef](#)]
173. Kiriker, G.R.; Shinde, V.; Schulz, M.J.; Sundaresan, M.J.; Hughes, S.; van Dam, J.; Nkrumah, F.; Grandhi, G.; Ghoshal, A. Monitoring multi-site damage growth during quasi-static testing of a wind turbine blade using a structural neural system. *Struct. Health Monit.* **2008**, *7*, 157–173. [[CrossRef](#)]
174. Blanch, M.J.; Dutton, A.G. Acoustic emission monitoring of field tests of an operating wind turbine. *Key Eng. Mater.* **2003**, *245*, 475–482. [[CrossRef](#)]
175. Papasalouros, D.; Tsopeles, N.; Anastasopoulos, A.; Kourousis, D.; Lekou, D.J.; Mouzakis, F. Acoustic emission monitoring of composite blade of NM48/750 NEG-MICON wind turbine. *J. Acoust. Emiss.* **2013**, *36*, 1.
176. Rumsey, M.A.; Paquette, J.A. Structural health monitoring of wind turbine blades. *Smart Sens. Phenom. Technol. Netw. Syst.* **2008**, 6933, 69330E. [[CrossRef](#)]
177. Berg, J.C.; Resor, B.R.; Paquette, J.A.; White, J.R. SANDIA REPORT SMART Wind Turbine Rotor: Design and Field Test; SAND2014-0681 6678; U.S. Department of Energy: Washington, DC, USA, 2014.
178. Hyers, R.W.; McGowan, J.G.; Sullivan, K.L.; Manwell, J.F.; Syrett, B.C. Condition monitoring and prognosis of utility scale wind turbines. *Energy Mater.* **2006**, *1*, 187–203. [[CrossRef](#)]
179. Ozbek, M.; Meng, F.; Rixen, D.J. Challenges in testing and monitoring the in-operation vibration characteristics of wind turbines. *Mech. Syst. Signal Process.* **2013**, *41*, 649–666. [[CrossRef](#)]
180. Hwang, S.; An, Y.-K.; Sohn, H. Continuous line laser thermography for damage imaging of rotating wind turbine blades. *Procedia Eng.* **2017**, *188*, 225–232. [[CrossRef](#)]

181. Amenabar, I.; Mendikute, A.; López-Arraiza, A.; Lizaranzu, M.; Aurrekoetxea, J. Comparison and analysis of non-destructive testing techniques suitable for delamination inspection in wind turbine blades. *Compos. Part B Eng.* **2011**, *42*, 1298–1305. [[CrossRef](#)]
182. Guo, P.; Infield, D. Wind turbine tower vibration modeling and monitoring by the nonlinear state estimation technique (NSET). *Energies* **2012**, *5*, 5279–5293. [[CrossRef](#)]
183. Kusiak, A.; Zhang, Z. Analysis of wind turbine vibrations based on SCADA data. *J. Sol. Energy Eng.* **2010**, *132*, 0310081–03100812. [[CrossRef](#)]
184. Andrew Swartz, R.; Lynch, J.P.; Zerbst, S.; Sweetman, B.; Rolfes, R. Structural monitoring of wind turbines using wireless sensor networks. *Smart Struct. Syst.* **2010**, *6*, 183–196. [[CrossRef](#)]
185. Kilic, G.; Unluturk, M.S. Testing of wind turbine towers using wireless sensor network and accelerometer. *Renew. Energy* **2015**, *75*, 318–325. [[CrossRef](#)]
186. Smarsly, K.; Hartmann, D. Structural health monitoring of wind turbines observed by autonomous software components—2nd level monitoring. In Proceedings of the 14th International Conference on Computing in Civil and Building Engineering, Moscow, Russia, 27–29 June 2012.
187. Smarsly, K.; Hartmann, D.; Law, K.H. A Computational framework for life-cycle management of wind turbines incorporating structural health monitoring. *Struct. Health Monit.* **2013**, *12*, 359–376. [[CrossRef](#)]
188. Smarsly, K.; Hartmann, D.; Law, K.H. An integrated monitoring system for life-cycle management of wind turbines. *Smart Struct. Syst.* **2013**, *12*, 209–233. [[CrossRef](#)]
189. Rolfes, R.; Zerbst, S.; Haake, G.; Reetz, J.; Lynch, J.P. Integral SHM-System for Offshore Wind Turbines Using Smart Wireless Sensors. In Proceedings of the International Workshop on Structural Health Monitoring, Stanford, CA, USA, 11–13 September 2007; pp. 1–8.
190. Fritzen, C.-P.; Kraemer, P.; Klinkov, M. An Integrated SHM Approach for Offshore Wind Energy Plants Introduction: Short Overview of Monitoring Systems for OWEP. In Proceedings of the IMAC-XXVIII, Jacksonville, FL, USA, 1–4 February 2011.
191. Faulkner, P.; Cutter, P.; Owens, A. Structural Health Monitoring Systems in Difficult Environments-Offshore Wind Turbines. In Proceedings of the 6th European Workshop on Structural Health Monitoring, Dresden, Germany, 2–3 February 2012.
192. Devriendt, C.; Magalhães, F.; El Kafafy, M.; De Sitter, G.; Cunha, Á.; Guillaume, P. Long-term dynamic monitoring of an offshore wind turbine. In *Topics in Dynamics of Civil Structures, Volume 4, Proceedings of the 31st IMAC, A Conference on Structural Dynamics*; Springer: Berlin/Heidelberg, Germany, 2013; pp. 253–267. [[CrossRef](#)]
193. Wind Farm Fears as Blade Snaps | The Times. Available online: <https://www.thetimes.co.uk/article/wind-farm-fears-as-blade-snaps-gd9wg90wwns> (accessed on 18 August 2021).
194. Yang, W.; Peng, Z.; Wei, K.; Tian, W. Structural health monitoring of composite wind turbine blades: Challenges, issues and potential solutions. *IET Renew. Power Gener.* **2017**, *11*, 411–416. [[CrossRef](#)]
195. Ou, Y.; Grauvogel, B.; Spiridonakos, M.; Dertimanis, V.; Chatzi, E.; Vidal, J. Vibration-based damage detection on a blade of a small scale wind turbine. In Proceedings of the 10th International Workshop on Structural Health Monitoring IWSHM 2015, Porto, Portugal, 1–3 September 2015. [[CrossRef](#)]
196. Wei, J.; McCarty, J. Acoustic emission evaluation of composite wind turbine blades during fatigue testing on JSTOR. *JSTOR* **1993**, *17*, 266–274.